Chapter 3

Oxidation of Pure Metals

Reaction of a pure metal with a single oxidant (oxygen, carbon, nitrogen, sulphur or a halogen) is considered. Most metals present in alloys used at high temperature form solid oxides, carbides or nitrides, but sulphides have lower melting points than the corresponding oxides, and liquid formation must sometimes be considered. We commence by surveying a selected set of experimental findings. The goal is to follow the development of a theoretical framework devised to provide an understanding of those findings, and which can be used as a predictive basis for corrosion rates under different conditions.

3.1 EXPERIMENTAL FINDINGS

Cross-sections of oxide scales grown on iron, cobalt, nickel and chromium are compared in Fig. 3.1, and the complex sulphide scale grown on cobalt is shown in Fig. 3.2. All of these scales were found to thicken according to parabolic kinetics,

$$X^2 = 2k_p t \qquad [3.1]$$

a result seen earlier to correspond to rate control by diffusion through the scale. It is to be expected then that the relative rates would correspond to the

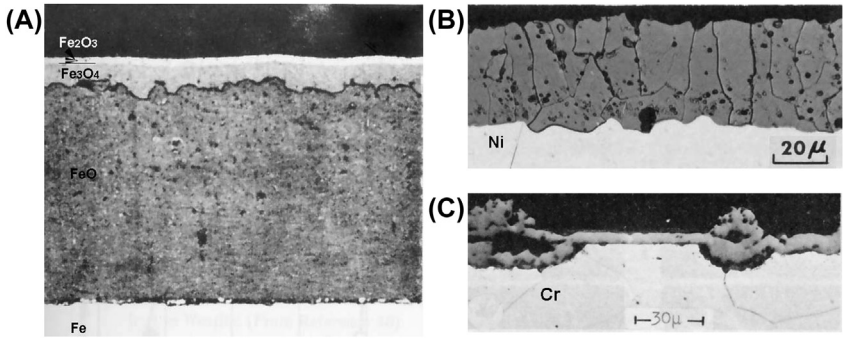

FIGURE 3.1 Cross-sections of oxide scales on (A) Fe *(Reprinted from J. Paidassi, Rev. Met. 54 (1957) 569, with permission from La Revue de Metallurgie.)*, (B) Ni *(Reproduced with permission from D. Caplan, M.J. Graham, M. Cohen, J. Electrochem. Soc. 119 (1972) 1205, The Electrochemical Society.)*, and (C) Cr. *(Reprinted with kind permission from D. Caplan, G.I. Sproule, Oxidation Met. 9 (1975) 459, Springer Science and Business Media.)*

High Temperature Oxidation and Corrosion of Metals. http://dx.doi.org/10.1016/B978-0-08-100101-1.00003-0

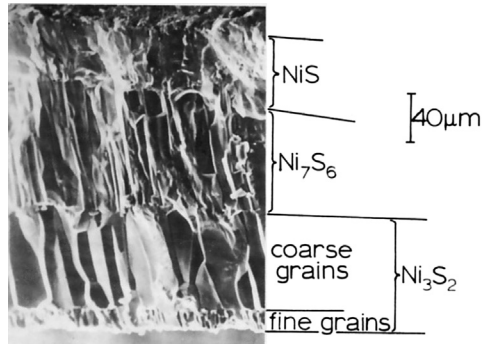

FIGURE 3.2 Fracture cross-section of sulphide scale on Ni. *Reprinted with kind permission from T. Narita, K. Nishida, Trans. Jpn. Inst. Met. 14 (1973) 439, 447, Springer Science and Business Media.*

TABLE 3.1 Selected Scaling Parabolic Rate Constants, k_p ($cm^2\ s^{-1}$)

Metal	Gas	T (°C)	k_p	References
Fe	Air (1 atm)	1000	2×10^{-7}	[1]
Co	O_2 (1 atm)	1000	3.3×10^{-9}	[2]
Ni	O_2 (1 atm)	1000	9×10^{-11}	[3]
Cr	O_2 (1 atm)	1000	6×10^{-14}	[4]
Fe	S_2 (1 atm)	900	7×10^{-6}	[5]
Co	S_2 (1 atm)	700	2×10^{-7}	[6]

nature of the oxides. Representative values of k_p are summarised in Table 3.1. Under the conditions examined, the scale grown on iron is approximately 95% FeO, 4% Fe_3O_4 and 1% Fe_2O_3 [1]. To a reasonable approximation, then, the k_p value for iron oxidation represents the growth of the FeO layer. Noting that FeO, CoO and NiO all have the same crystal structure (isotypic with face-centred-cubic NaCl) it is seen that their growth rates, nonetheless, differ widely. The Cr_2O_3 phase has a hexagonal crystal structure and is therefore not to be compared on this basis with the cubic oxides. Finally, it is seen that iron sulphidises much more rapidly than it oxidises.

The rate constant values in Table 3.1 are for specific temperatures and pressures. It is common that the temperature dependence can be described by the Arrhenius relationship

$$k_p = k_o \exp(-Q/RT) \qquad [3.2]$$

where Q is a constant known as the effective activation energy and k_o is also a constant. As seen in Table 3.2, values of Q and k_o differ widely from one metal

TABLE 3.2 Arnhenius Activation Energy (Eq. [3.2]) for Oxide Scale Growth

Metal/Gas	T (°C)	Q (kJ mol^{-1})	References
Fe/O_2	700–1000	164	[1]
Co/O_2	800–950 950–1150	230 150	[2]
Ni/O_2	600–1100 1100–1400	120 240	[3]
Cr/O_2	980–1200	243	[4]

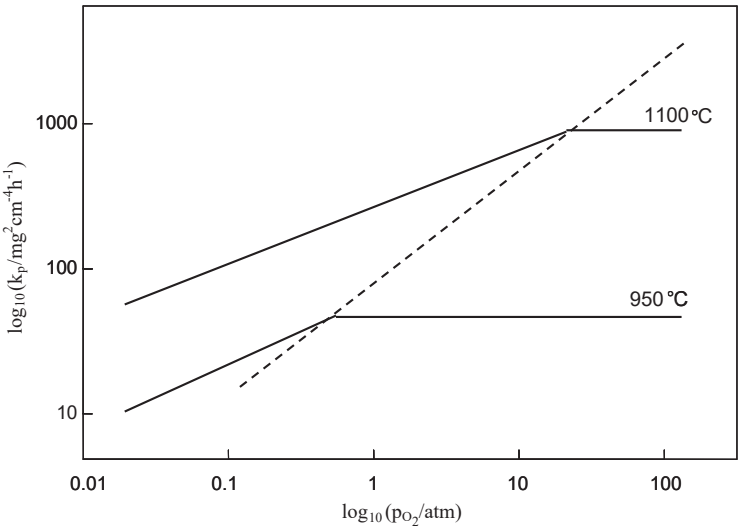

FIGURE 3.3 Oxygen partial pressure effects on k_p for cobalt. *Data from D.W. Bridges, J.P. Baur, W.M. Fassel, J. Electrochem. Soc. 103 (1956) 619.*

to another. In some cases, different values apply for the same metal in different temperature regimes.

An example of the oxygen pressure effect on k_p is shown in Fig. 3.3. The linearity of the log–log plots demonstrates the applicability of the relationship

$$k_p = k_o p_{O_2}^{\frac{1}{n}} \qquad [3.3]$$

where k_o, n are constants.

In order to properly account for these observations, it is necessary to analyse more carefully the diffusion processes which support scale growth and determine their rates. Such an analysis was first carried out by Wagner [9], and we follow his treatment here, rephrasing it in terms of the Kroger-Vink description [10] of the defect solid state.

A central assumption of Wagner's theory of scale growth is that the process is supported by diffusion of crystalline lattice species through the scale. Thus the oxide is considered to be compact and free of pores and cracks. Any effect of grain boundaries and other extended defects is ignored, and attention is focused on the movement of individual lattice site, or 'point', defects. The nature of these defects is considered first, and the relationship between defect concentration and oxide nonstoichiometry is developed. A technique of grouping point defects as 'structural units' is used to relate micro and macroscopic levels of thermodynamic description. Point defect diffusion is then described, and its use in the classical Wagner treatment explored. The utility of this description in accounting for experimental observations is then examined. Finally, the limitations of this treatment are identified, and their consequences for scale growth kinetics are examined.

3.2 USE OF PHASE DIAGRAMS

The Wagner theory describes steady-state kinetics, controlled by diffusion within a scale under fixed boundary conditions. Thus the chemical potentials of diffusing species at the metal-scale, scale-gas and any intermediate interfaces are supposed to be time invariant. In this event, local equilibrium will be in effect at those boundaries, which should therefore correspond to boundaries defined by the metal-oxidant phase diagram. A first step in verifying that a scaling reaction is diffusion controlled is to test the validity of this proposition.

We saw earlier that the three-layered oxide scale grown on iron at temperatures above 570°C was as predicted from the Fe-O phase diagram (Fig. 2.2). A more quantitative test is possible with sulphides, because electron probe microanalysis (EPMA) can be used to measure both metal and oxidant concentrations at precisely defined (±1 μm) locations within a scale. Results obtained by Bastow and Wood [7] for the nickel sulphide scale are compared with the Ni-S phase diagram in Fig. 3.4, where agreement is seen to be good.

In the case of reaction products with significant deviations from stoichiometry, their composition will vary with position within the scale, from the metal-rich to the oxidant-rich sides of the oxide field defined by the phase diagram. This is easier to measure in sulphides than in oxides, because of the greater sensitivity of the EPMA technique to the high atomic weight sulphur. Results for an $Fe_{1-\delta}S$ scale in Fig. 3.4C show that the expected compositional gradient was indeed developed [8].

3.3 POINT DEFECTS AND NONSTOICHIOMETRY IN IONIC OXIDES

For isothermal diffusion in the absence of external fields, there is no net flow of charge. Any physically realistic mechanism must therefore involve the movement of groups of species which conserve charge and, of course, sites. As

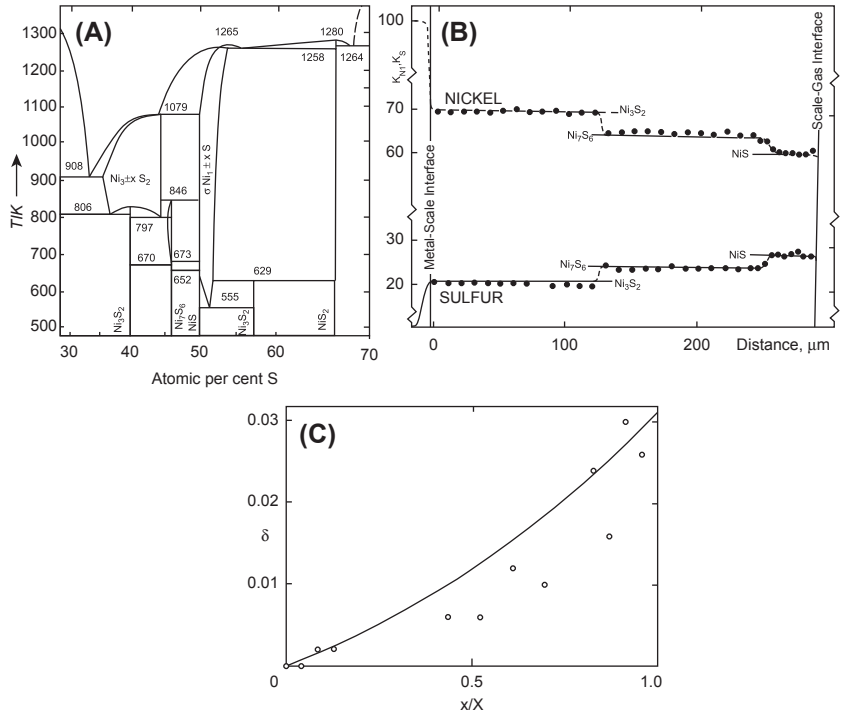

FIGURE 3.4 (A) Phase diagram for Ni-S system; (B) microanalysis of compositional variation in sulphide scale on Ni at 448°C *(With kind permission from B.D. Bastow, G.C. Wood, Oxid. Met. 9 (1975) 473, Springer Science and Business Media.)*; (C) microanalysis of deviation from stoichiometry in $Fe_{1-\delta}$-S scale grown on Fe at 700°C *(Reproduced with permission from D.J. Young, W.W. Smeltzer, J. Electrochem. Soc. 123 (1976) 232, The Electrochemical Society)*.

will be demonstrated in the next section, such groups fit the definition of 'relative building units' conceived of by Kroger et al. [11] in the development of a thermodynamic description of point defect equilibria. Since these units can be used to represent both diffusion and equilibrium, they form an appropriate link between the transport properties and local equilibrium state of a solid.

In what follows, we employ the defect notation of Kroger and Vink [10] wherein the oxide lattice species are represented by the symbol $S_M^{\times}$. Here the subscript represents the normal occupancy in a perfect crystal of the site in question, and the principal symbol represents the species actually occupying the site. The superscript represents the charge of the species relative to normal site occupancy with a prime indicating a negative, a dot positive and a cross zero charge. Thus, for example, the principal lattice species in magnesiowüstite, (Fe,Mg)O, are the two cations $Fe_{Fe}^{\times}$, $Mg_{Fe}^{\times}$ and the anion $O_O^{\times}$. Defect species are now introduced.

Following the early work of Frenkel [12] Schottky and Wagner [13] and Jost [14], we consider first the lattice defects, which can arise in a homogeneous, crystalline ionic solid. Firstly, individual lattice sites can be vacant. In a binary oxide MO, the possibilities are $V_M^{\times}$, V_M' and V_M'', representing different ionisation states, on the cation sublattice, plus $V_O^{\times}$, etc. on the anion sublattice. In addition, interstitial species, eg, $M_i^{\bullet\bullet}$ and O_i'', are possible, with the subscript i denoting an interstitial lattice site. Interstitial oxygen is unusual, because its large size makes interstitial occupancy energetically improbable in most oxides. The formation of charged defects always occurs in matching sets, to balance electrostatic charge. Schottky defects consist of cation and anion vacancies, eg, $V_{Ni}'' + V_O^{\bullet\bullet}$ in nickel oxide. Frenkel defects consist of matched vacancies and interstitials, eg, $V_{Cd}'' + Cd_i^{\bullet\bullet}$ in CdO and $V_O^X + O_i^X$ in UO_2.

As seen in Section 2.2, defects of this sort always exist at temperatures above 0 K. However, their existence does not account for nonstoichiometry in oxides, for example, the large deviations from stoichiometry observed in $Fe_{1-\delta}O$ (Fig. 2.2). In fact, that particular system is complicated by interactions between the highly concentrated defects. We consider instead deviations from stoichiometry in a model oxide $M_{1-\delta}O$ in which it is assumed fully ionised cation and anion vacancies can form. Using equilibrium expressions of the form of Eq. [2.106] we write the Schottky reaction

$$0 = V_M'' + V_o^{\bullet\bullet} \qquad [3.4]$$

for which

$$K_S = n_{V_M} n_{V_O} / N^2 \qquad [3.5]$$

with K_S the Schottky equilibrium constant and $N = n + n_v$, the total number of sites on each sublattice, N_M and N_O, which are here taken as equal for a divalent metal oxide.

Deviations from stoichiometry are achieved by the interchange of matter, usually oxygen, with the surrounding environment. In the metal deficit ($\delta > 0$) range

$$\frac{1}{2}O_2(g) = O_O^{\times} + V_M'' + 2h^{\bullet} \qquad [3.6]$$

and

$$K_P = n_{V_M} n_h^2 / N^3 p_{O_2}^{\frac{1}{2}} \qquad [3.7]$$

whilst in the metal excess ($\delta < 0$) range

$$O_O^{\times} = V_O^{\bullet\bullet} + 2e' + \frac{1}{2}O_{2(g)} \qquad [3.8]$$

$$K_N = n_{V_O} n_e^2 p_{O_2}^{\frac{1}{2}} \Big/ N^3 \qquad [3.9]$$

Here K_P, K_N are equilibrium constants, e' is an electron and $h^{\bullet}$ a positive hole: the metal excess oxide exhibits n-type semiconductivity and the metal deficit oxide shows p-type behaviour.

It is noted in formulating these equations that sites can be created or destroyed, as in Eq. [3.6], but the crystalline phase is preserved by maintaining the site ratio N_M/N_O constant, unity in this case. Mass is conserved, effective charge is conserved and the electroneutrality of the compound is always preserved. Note also that adoption of the 'effective charge' description means that charge is associated only with defect species. This avoids the clumsiness of counting ions and comparing large numbers ($\sim 10^{22}$ cm^{-3}) to arrive at very small differences.

The relationship between intrinsic disorder, ie, the concentration of defects when $\delta = 0$, extent of nonstoichiometry and p_{O_2} is of interest. The deviation from stoichiometry is

$$\delta = (n_{V_M} - n_{V_O})/N \qquad [3.10]$$

The vacancy concentrations are found from Eqs [3.7] and [3.9] using the approximations

$$n_h = 2n_{V_M} \qquad [3.11]$$

$$n_e = 2n_{V_O} \qquad [3.12]$$

for charge balance in the relevant regimes, and their substitution into Eq. [3.10] yields

$$\delta = \left(\frac{K_P}{4}\right)^{\frac{1}{3}} p_{O_2}^{\frac{1}{6}} - \left(\frac{K_N}{4}\right)^{\frac{1}{3}} p_{O_2}^{-\frac{1}{6}} \qquad [3.13]$$

This is the desired relationship between nonstoichiometry and p_{O_2}. We now relate it to the conditions for stoichiometry.

Defining $p_{O_2}^{(o)}$ as the equilibrium partial pressure at which the compound is stoichiometric, $\delta = 0$, we find from Eq. [3.13] that

$$K_N = K_p p_{O_2}^{(o)} \qquad [3.14]$$

When $\delta = 0$, it follows from Eqs [3.5] and [3.10] that the intrinsic disorder, Δ, is given by

$$\Delta = \frac{n_{V_M}^{(o)}}{N} = \frac{n_{V_O}^{(o)}}{N} = K_S^{\frac{1}{2}} \qquad [3.15]$$

Combination of Eqs [3.5], [3.7] and [3.9] leads to

$$K_P K_N = K_S K_e^2 \qquad [3.16]$$

where

$$K_e = n_h n_e$$

corresponding to the electron–hole pair formation equilibrium

$$0 = h^{\bullet} + e' \qquad [3.17]$$

Substitution from Eqs [3.14] and [3.16] into Eq. [3.13] yields

$$\delta = K_S^{\frac{1}{6}}\left(\frac{K_e}{4}\right)^{\frac{1}{3}}\left\{\left(\frac{p_{O_2}}{p_{O_2}^{(o)}}\right)^{\frac{1}{6}} - \left(\frac{p_{O_2}^{(o)}}{p_{O_2}}\right)^{\frac{1}{6}}\right\} \qquad [3.18]$$

which upon substitution from Eq. [3.15] leads to

$$\delta = \left(\frac{\Delta K_e}{4}\right)^{\frac{1}{3}}\left\{\left(\frac{p_{O_2}}{p_{O_2}^{(o)}}\right)^{\frac{1}{6}} - \left(\frac{p_{O_2}^{(o)}}{p_{O_2}}\right)^{\frac{1}{6}}\right\} \qquad [3.19]$$

As pointed out by Greenwood [15], this general description reveals that the greater the intrinsic disorder, Δ, of the stoichiometric compound, the smaller is the *relative* partial pressure change required to produce a given deviation from stoichiometry. Conversely, oxides which are close to stoichiometric have low Δ values. This is true despite the fact that compounds with the same defect type will evidence the same functional relationship between x and p_{O_2}. The applicability of equations like Eq. [3.19] is, of course, limited to the oxide phase field, and can be of even narrower applicability if defect interactions become important. It is clear from [Eq. 3.19] that an oxygen potential gradient across an oxide scale gives rise to a defect concentration gradient. It is this gradient which provides the mechanism for diffusion through an oxide scale bounded on one side by metal and on the other by oxygen gas. An example is shown in Fig. 3.4C.

3.4 LATTICE SPECIES AND STRUCTURAL UNITS IN IONIC OXIDES

Consider a p-type oxide MO, containing fully ionised vacancies and positive holes, under isothermal, isobaric conditions. The lattice species are

$$M_M^{\times}, V_M'', h^{\bullet}, O_O^{\times}$$

and thus outnumber the single thermodynamically independent compositional variable available to the binary oxide. The removal of the dependencies among the set is accomplished by the application of the physical constraints which exist for the species. In a crystalline solid the ratio of cation to anion sites is fixed

$$n\left(M_M^{\times}\right) + n\left(V_M''\right) = n\left(O_O^{\times}\right) \qquad [3.20]$$

and, in the absence of a field, the system is charge neutral

$$2n\left(V_M''\right) + n\left(h^{\bullet}\right) = 0 \qquad [3.21]$$

The use of these relationships has been explored by Kroger et al. [11] in arriving at their definition of building units. Building units are groups of lattice species with such a composition that the requirements Eqs [3.20] and [3.21] are met when the group is added to the crystal. The obvious unit for MO is $\left\{M_M^{\times} + O_0^{\times}\right\}$. A subset of building units is comprised of 'relative building units'. These are defined relative to the perfect crystal and consist of the difference between a lattice species and the lattice species corresponding to normal site occupancy. Thus relative building units represent a change in composition resulting from the replacement of one species with another, eg, $\left\{B_M^{\times} - A_M^{\times}\right\}$ in a substitutional solid solution.

Since relative building units represent compositional change, they can be used to describe diffusion. It is clear that a flux of unit $\left\{B_M^{\times} - A_M^{\times}\right\}$ corresponds to interdiffusion of cations A and B via a site-exchange process. The formulation of suitable relative building units emerges from the flux constraints, which are analogous to the site and charge density constraints Eqs [3.20] and [3.21]. In the case of one-dimensional diffusion in the model system under discussion, these constraints are, for a ternary oxide,

$$J_A + J_B + J_V = 0 = J_0 \qquad [3.22]$$

$$2J_V = J_h \qquad [3.23]$$

where the fluxes, J, are measured within the solvent-fixed reference frame provided by an immobile anion lattice. It follows that movement of a vacancy must be accompanied by movement of positive holes and is associated with an opposing flux of cations. Relative building units, U_i, which describe these exchanges are:

$$U_1 \equiv \left\{A_M^{\times} - V_M'' - 2h^{\cdot}\right\} \qquad [3.24]$$

$$U_2 \equiv \left\{B_M^{\times} - V_M'' - 2h^{\cdot}\right\} \qquad [3.25]$$

$$U_3 \equiv \left\{B_M^{\times} - A_M^{\times}\right\} \qquad [3.26]$$

of which one unit is seen to be redundant. A further unit not contributing to diffusion but necessary to complete the structure is

$$U_4 \equiv \left\{O_O^{\times} - V_M'' - 2h^{\cdot}\right\} \qquad [3.27]$$

It is clear that combination in the appropriate proportions of units 1, 2 and 4 yield a solid (A,B)O of any desired degree of substitution and nonstoichiometry.

Thermodynamic meaning is now attached to the relative building units by considering the reactions which lead to the introduction of point defects into the compound:

$$A_{(g)} + V_M'' + 2h^{\cdot} = A_M^{\times} \qquad [3.28]$$

$$B_{(g)} + V''_M + 2h^{\bullet} = B^{\times}_M \quad [3.29]$$

$$O^{\times}_O + V''_M + 2h^{\bullet} = \frac{1}{2}O_{2(g)} \quad [3.30]$$

These equilibria are described by their corresponding Gibbs equations which, under isothermal field-free conditions, may be written in terms of molar concentrations, m, and electrochemical potentials, η, as

$$\sum_i \eta_i dm_i = 0$$

in each case. Since the dm_i are related via the reaction stoichiometry coefficients, v, we may write

$$\sum_i \nu_i \eta_i = 0 \quad [3.31]$$

whence

$$\mu_A = \eta(A_M) - \eta\left(V''_M\right) - 2\eta(h^{\bullet}) = \mu(U_1) \quad [3.32]$$

$$\mu_B = \eta(B_M) - \eta\left(V''_M\right) - 2\eta(h^{\bullet}) = \mu(U_2) \quad [3.33]$$

$$\frac{1}{2}\mu_{O_2} = \eta(O_o) + \eta\left(V''_M\right) + 2\eta(h^{\bullet}) = \mu(U_3) \quad [3.34]$$

and the potentials of U_1, U_2 and U_4 are seen to be the chemical potentials of the constituent elements, μ_i. The electrochemical potentials of individual lattice species cannot be measured. Moreover, they depend on the local electrostatic potential, ψ, through the definition

$$\eta(S^z) = \mu(S^z) + zF\psi$$

where z is the effective charge of the species and F is the Faraday. The value of ψ is also inaccessible to measurement. It is apparent that appropriate grouping of species leads to the avoidance altogether of the need to directly consider the electrostatic potential or individual species chemical potentials. These quantities are indeterminate within the formalism, just as they are experimentally inaccessible.

Since it is not possible to add, remove or diffuse lattice species other than in a way which conserves charge and lattice sites, the use of relative building units is entirely consistent with the fact that the thermodynamics and diffusion kinetics of ionic crystals can always be described in terms of elemental chemical potentials. Relative building units provide a link between the macroscopic thermodynamic/kinetic properties and the point defect structure.

3.5 GIBBS–DUHEM EQUATION FOR DEFECTIVE SOLID OXIDES

For an isothermal, isobaric and chemically equilibrated system, the Gibbs–Duhem equation [2.46] (in Chapter 2)

$$\sum_i n_i d\mu_i = 0$$

relates the chemical potentials of the constituent elements. The relationship applies to an open system, ie, one which can exchange matter with its surroundings. It is therefore appropriate to the case of a solid oxide which achieves equilibrium via the transfer of oxygen to or from the ambient gas phase. As we have seen, such an oxide is generally nonstoichiometric, its composition varying continuously with oxygen activity. Such an oxide may be regarded as a solution composed of an oxide of chosen reference composition and an excess amount of one constituent.

We consider here a pure binary metal-deficit oxide of composition $M_{1-\delta}O$. It is frequently convenient, if not always realistic, to adopt as a reference the stoichiometric composition MO. The formation of the metal-deficit oxide solution may then be represented as

$$(1-\delta)\mathrm{MO(s)} + (\delta/2)\mathrm{O_2(g)} = \mathrm{M_{1-\delta}O(s)}$$

Although one cannot write a Gibbs equilibrium equation for this, or any other, solution formation process (because the composition of the product varies with a_o), the Gibbs–Duhem equation is clearly of the form

$$(1-\delta)d\mu_{\mathrm{MO}} + \delta d\mu_{\mathrm{o}} = 0 \qquad [3.35]$$

This result informs us that the chemical potential of the reference composition oxide varies with oxygen activity. Alternatively, one might consider the solution $M_{1-\delta}O$ as being formed from its elements and write

$$(1-\delta)d\mu_{\mathrm{M}} + d\mu_O = 0 \qquad [3.36]$$

The alternative expressions given by Eqs [3.35] and [3.36] are linked via the statement of equilibrium for formation of the reference oxide

$$\mathrm{M(s)} + 1/2\mathrm{O_2(g)} = \mathrm{MO(s)}$$

the Gibbs equation for which is

$$d\mu_{\mathrm{M}} + d\mu_{\mathrm{O}} = d\mu_{\mathrm{MO}} \qquad [3.37]$$

Since the Gibbs–Duhem equation represents the means of removing redundancy among a set of chemical potentials, it need not have a unique form. The several different, but equivalent, forms of the equation are related by the equilibria which exist among the various chemical species.

Similarly, it is possible to write the Gibbs–Duhem equation in terms of lattice and defect species because the electrochemical potentials of the species are related via the appropriate building units to the chemical potentials of the elements. Thus substitution of the relationships Eqs [3.32] and [3.34] for doubly changed vacancies in a binary oxide MO into Eq. [3.36] leads immediately to

$$(1-\delta)d\eta\left(\mathrm{M}_{\mathrm{M}}^{X}\right)+d\eta\left(\mathrm{O}_{\mathrm{O}}^{\times}\right)+\delta d\eta\left(V_{\mathrm{M}}''\right)+2\delta d\eta(h)=0 \qquad [3.38]$$

It follows from the site and charge balances of Eqs [3.20] and [3.21] that

$$\delta=n\left(V_{\mathrm{M}}''\right)/n\left(O_{\mathrm{O}}^{\times}\right) \qquad [3.39]$$

$$1-\delta=n\left(\mathrm{M}_{\mathrm{M}}^{\times}\right)/n\left(\mathrm{O}_{\mathrm{O}}^{\times}\right) \qquad [3.40]$$

Substitution from Eqs [3.39], [3.40] and [3.21] into Eq. [3.38] then yields

$$n\left(\mathrm{M}_{\mathrm{M}}^{\times}\right)d\eta\left(\mathrm{M}_{\mathrm{M}}^{\times}\right)+n\left(\mathrm{O}_{\mathrm{O}}^{\times}\right)d\eta\left(\mathrm{O}_{\mathrm{O}}^{\times}\right)+n\left(V_{\mathrm{M}}''\right)d\eta\left(V_{\mathrm{M}}''\right)+2n(h^{\bullet})d\eta(h^{\bullet})=0 \qquad [3.41]$$

which is the form appropriate to individual species. The elemental form Eq. [3.36] and the lattice species form Eq. [3.41] of the Gibbs–Duhem equation are completely consistent. This is a necessary consequence of the imposed condition of local equilibrium expressed through Eqs [3.32] and [3.34]. Similar analyses can be performed for other defect types, with the same general conclusion being reached [17].

3.6 LATTICE DIFFUSION AND OXIDE SCALING: WAGNER'S MODEL

Wagner's original treatment [9,16] was of critical importance in providing an understanding of the particle (atomic or ionic) processes occurring within a growing oxide scale, thereby leading to a capacity to predict the effects on the oxidation rate of changes in temperature, oxide chemistry, etc. The treatment is based on the assumption that lattice diffusion of ions or the transport of free carriers (electrons or positive holes) controls scaling rates. For diffusion to be rate controlling, the scale boundaries must achieve local equilibrium. This requires that the processes occurring at the metal-scale and scale-gas interfaces are so fast that they do not contribute to rate control and may be regarded as at equilibrium. Although this will not be the case at the very beginning of a reaction, equilibrium is quickly established once a continuous scale is formed, providing that the supply of gaseous oxidant is abundant.

If diffusion by lattice species is to be rate controlling, then no other diffusion process can contribute significantly to mass transfer. Thus the scale must be dense (ie, nonporous) and adherent to the metal, so that gas-phase transport within the scale is unimportant. Furthermore the scale must contain a relatively low density of grain boundaries and dislocations so that their contribution to diffusion is unimportant, and the oxide lattice (or volume) diffusion properties dictate mass transfer rates.

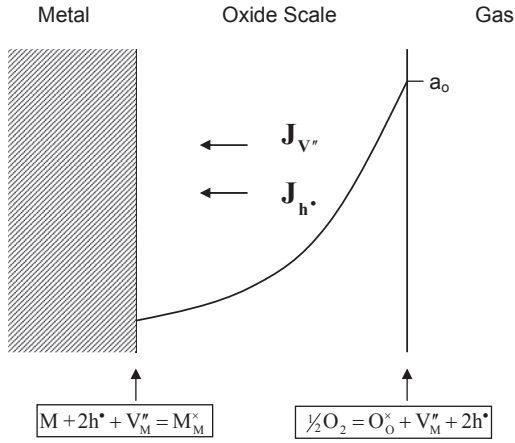

FIGURE 3.5 Schematic view of Wagner's diffusion model for cation vacancy transport.

The Wagner model is illustrated in Fig. 3.5 for the more common case of cation transport. Oxygen anion transport can sometimes occur, usually via vacancy movement. In his original model, Wagner proposed that ions and electronic species migrated independently. This is correct only to the extent that (1) charge separation can be sustained within the oxide, and (2) the oxide is thermodynamically and kinetically ideal, so that the cross-terms in a complete diffusion description (Eq. [2.99]) can be ignored. The latter point has been made by Wagner [18] and others [19,20].

Wagner solved the transport problem by writing two equations, for ionic and electron species, in terms of their electrochemical potential gradients. These were of the form Eq. [2.99] without cross-terms and written in terms of mobilities, B_i:

$$J_i = -C_i B_i \nabla \eta_i \qquad [3.42]$$

Here the species mobility is defined as its drift velocity under an electrochemical potential gradient of unity. A comparison of Eq. [3.42] and Eq. [2.99] yields

$$L_{11} = C_1 B_1 \qquad [3.43]$$

when cross-terms are ignored. If, furthermore, the system is field free (as in, for example, a tracer diffusion experiment) and thermodynamically ideal, we have from Eq. [2.103]

$$D_1 = L_{11} RT / C_1 \qquad [3.44]$$

whence

$$B_1 RT = D_1 \qquad [3.45]$$

a form of the Nernst–Einstein relationship between diffusion and mobility.

Consider the growth of a p-type (metal deficit) binary oxide scale sustained by metal vacancy diffusion. Writing Eq. [3.42] explicitly, one obtains

$$J_V = -C_V B_V \left(\frac{\partial \mu_{\mathrm{i}}}{\partial x} + 2FE \right) \qquad [3.46]$$

$$J_h = -C_h B_h \left(\frac{\partial \mu_h}{\partial x} - FE \right) \qquad [3.47]$$

where the electrostatic field

$$E = -\frac{d\psi}{dx} \qquad [3.48]$$

and the effective charges $z_v = -2$, $z_h = 1$ have been inserted. The difficulty is that the local electrostatic field cannot be measured. Recognising that any field developed by charge within the oxide would affect the flux of other charged species, Wagner resolved the problem by invoking the condition of zero net electric current Eq. [3.23]. In this way the unknown quantity E is eliminated between Eqs [3.46] and [3.47] via the result

$$E = \frac{1}{(B_h + 2B_V)F} \left\{ B_V \frac{\partial \mu_V}{\partial x} - B_h \frac{\partial \mu_h}{\partial x} \right\} \qquad [3.49]$$

Resubstitution in Eq. [3.46] leads to

$$J_V = -\frac{C_V B_V B_h}{B_h + 2B_V} \left\{ \frac{\partial \mu_V}{\partial x} + 2 \frac{\partial \mu_h}{\partial x} \right\} \qquad [3.50]$$

The expression in braces is related to thermodynamic variables via the local equilibrium Eq. [3.34], rewritten for a fixed anion lattice as

$$d\mu_{\mathrm{o}} = d\eta_V + 2d\eta_h \qquad [3.51]$$

Since $z_V = -2z_h$, the electrostatic potential terms on the right-hand side cancel, and Eq. [3.50] becomes

$$J_V = -\frac{C_V B_V B_h}{B_h + 2B_V} \frac{d\mu_o}{dx} \qquad [3.52]$$

As the mobilities of free carriers are usually much greater than those of ions, $B_h \gg B_V$ (and $B_e \gg B_{\mathrm{M_i}}$), this result is well approximated by

$$\begin{aligned} J_V &= -C_V B_V \frac{d\mu_o}{dx} \\ &= \frac{-C_V D_V}{RT} \frac{d\mu_o}{dx} \\ &= -C_V D_V \frac{d \ln a_o}{dx} \end{aligned} \qquad [3.53]$$

which is one form of Wagner's original solution.

The algebra leading to Eq. [3.53] is tedious and, in more complex systems, quite time-consuming. A simpler procedure is afforded by a description of diffusion in terms of relative building units (Section 3.4). The unit of relevance to a binary metal deficit oxide is $U_1 = \left\{M_M^X - V_M'' - 2h^{\bullet}\right\}$. As described earlier, the diffusion of these units necessarily satisfies site and charge balance and is equivalent to cation diffusion through the oxide.

$$\begin{aligned} J_M &= J(U_1) \\ &= -C_M B_M \frac{\partial}{\partial x}\left\{\eta\left(M_M^X\right) - \eta\left(V_M''\right) - 2\eta(h^{\bullet})\right\} \end{aligned} \quad [3.54]$$

Substitution from Eq. [3.32] leads immediately to

$$J_M = -C_M B_M \frac{d\mu_M}{dx} \quad [3.55]$$

which is transformed via the Gibbs–Duhem Eq. [3.36] to

$$J_M = \frac{C_M B_M}{1-\delta}\frac{d\mu_o}{dx} \quad [3.56]$$

$$J_M = \frac{C_M D_M}{(1-\delta)}\frac{d\ln a_o}{dx} \quad [3.57]$$

Recognising that because of site conservation

$$C_V D_V = C_M D_M \quad [3.58]$$

it is seen that Eqs [3.53] and [3.57] are equivalent at low values of δ.

The remaining step in this description is the relating of scale-thickening rate to diffusive flux through

$$\frac{dX}{dt} = J_M V_M = \frac{k_p}{X} \quad [3.59]$$

where V_M is the volume of oxide formed per mole of metal. It follows from Eqs [3.57] and [3.59] that

$$k_p = \frac{D_M}{1-\delta}\frac{d\ln a_o}{dy} \quad [3.60]$$

where y is the normalised position coordinate, $y = x/X$. Upon integration from $x = 0$ to $x = X$ (ie, from one side to the other of the scale), this yields

$$k_p = \int_{a_o'}^{a_o''} D_M \frac{1}{1-\delta} d\ln a_o \quad [3.61]$$

where a_o', a_o'' represent the boundary values of the oxygen activity at the metal-scale and scale-gas interfaces. Use of the relationship for vacancies

$$z_M/|z_o| = 1/(1-\delta)$$

leads to the form

$$k_p = \int_{a'_o}^{a''_o} D_M \frac{Z_M}{|Z_o|} d \ln a_o \qquad [3.62]$$

which was Wagner's original equation for metal oxidation.

In the case of very small deviations from stoichiometry, $\delta \ll 1$ and $z_M/|z_o|$ is constant. In this case, Eq. [3.62] can be expressed with the help of Eq. [3.58] as

$$k_p = \frac{z_M}{|z_o|} \int_{a'_o}^{a''_o} D_V C_V d \ln a_o \qquad [3.63]$$

This useful form corresponds to Eq. [1.25] as is seen below.

3.7 VALIDATION OF WAGNER'S MODEL

Considerable effort has been expended in testing both the qualitative and quantitative accuracy of the Wagner description of scale growth kinetics. In the event, quantitative success was achieved in a satisfactory number of important cases: the oxidation of iron, nickel, cobalt and copper; and the sulphidation of iron and silver. A review of the practically important cases of FeO, NiO, CoO and FeS scale growth is instructive.

3.7.1 Oxidation of Nickel

Nickel forms only one oxide, NiO, which exhibits a small range of non-stoichiometry, about 10^{-3} at.% on the metal-deficit side. Although NiO scales are formed over a wide temperature range, it is only at temperatures above 900°C that the oxide grain size is sufficiently large for lattice diffusion to predominate over grain boundary transport.

Defect concentration and electrical and diffusional properties of NiO have been interpreted in terms of noninteracting cation vacancies:

$$\frac{1}{2}O_2(g) = O_O^{\times} + V'_{Ni} + h^{\cdot} \qquad [3.64]$$

$$V'_{Ni} = V''_{Ni} + h^{\cdot} \qquad [3.65]$$

Thus if $[V'_{Ni}] \gg [V''_{Ni}]$, the charge balance for the system is

$$[V'_{Ni}] = [h^{\cdot}]$$

and the equilibrium Eq. [3.64] yields

$$V'_{Ni} = K p_{O_2}^{\frac{1}{4}} \qquad [3.66]$$

Conversely, if $\left[V''_{Ni}\right] \gg \left[V'_{Ni}\right]$, we have

$$2\left[V''_{Ni}\right] = [h^{\cdot}] = (K')^{\frac{1}{3}} p_{O_2}^{\frac{1}{6}} \qquad [3.67]$$

Several investigations [21–23] have shown that the defect properties of NiO are functions of oxygen pressure between $p_{O_2}^{\frac{1}{4}}$ and $p_{O_2}^{\frac{1}{6}}$. For example, the self-diffusion coefficient of nickel in NiO was shown by Volpe and Reddy [21] to be proportional to $p_{O_2}^{\frac{1}{6}}$ at 1245°C and $p_{O_2}^{\frac{1}{4}}$ at 1380°C, as shown in Fig. 3.6.

The values of D_{Ni} given in Fig. 3.6 can be used in Eq. [3.62] to predict scaling rate constants. The procedure is the same for any oxide for which $z_M/|z_o|$ can be approximated as constant, and the form Eq. [3.63] used. Setting

$$C_V = K p_{O_2}^{\frac{1}{n}} \qquad [3.68]$$

and hence

$$D_V C_V = D^{o}_{Ni} p_{O_2}^{\frac{1}{n}} \qquad [3.69]$$

where D^{o}_{Ni} is the self-diffusion coefficient at $p_{O_2} = 1$ atm, we obtain

$$\begin{aligned} k_p &= D^{o}_{Ni} \int_{a'_o}^{a''_o} p_{O_2}^{\frac{1}{n}} d \ln p_{O_2} \\ &= D^{o}_{Ni} \int_{a'_o}^{a''_o} p_{O_2}^{\frac{1}{n-1}} dp_{O_2} \end{aligned} \qquad [3.70]$$

which upon integration yields

$$k_p = n D^{o}_{Ni} \left\{ \left(p''_{O_2}\right)^{\frac{1}{n}} - \left(p'_{O_2}\right)^{\frac{1}{n}} \right\} \qquad [3.71]$$

Rates measured at $p_{O_2} = 1$ atm are compared in Fig. 3.7 with values predicted from Eq. [3.71] using the D^{o}_{Ni} temperature dependence provided by Volpe and Reddy [21].

Thus quantitative success was achieved with a model based on mass transport via individual point defect species. It should be noted, however, that the Volpe and Reddy diffusion description employed here could not define the relative contributions of the singly and doubly charged vacancies. More seriously, the model fails badly at temperatures below 900°C, as seen in Fig. 3.7.

3.7.2 Oxidation of Cobalt

The monoxide CoO is also of the metal deficit type, and shows a much larger deviation from stoichiometry than NiO, about 1 at. %. A higher oxide, Co_3O_4, forms at sufficiently high p_{O_2}, but values greater than 1 atm are required at

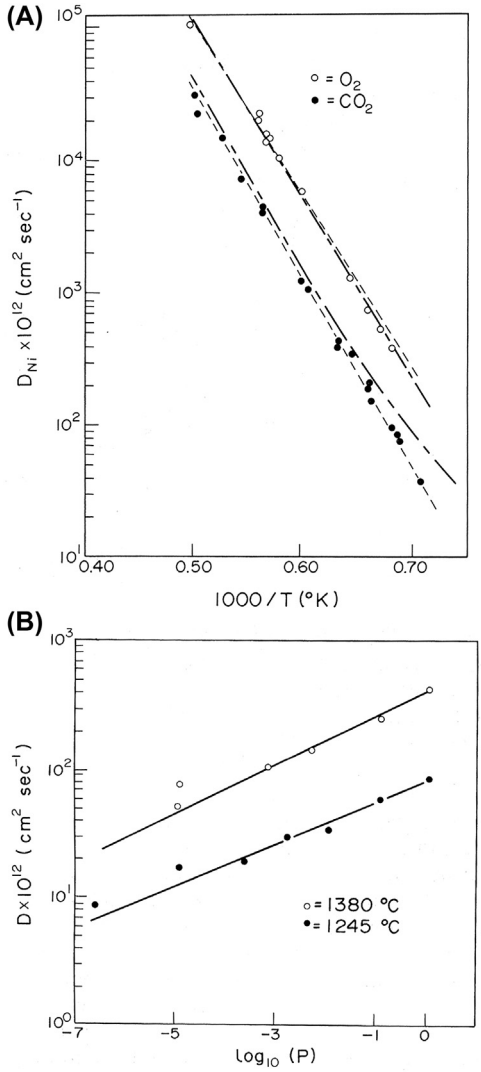

FIGURE 3.6 Self-diffusion coefficient of nickel in NiO (A) at 1 atm pressure as a function of temperature and (B) as a function of oxygen pressure. *Reproduced with permission from M.L. Volpe, J. Reddy, J. Chem. Phys. 53 (1970) 1117, copyright 1970, American Institute of Physics.*

$T > 900°C$. Growth of a single-phase CoO scale occurs via cobalt diffusion, as $D_o \sim 10^{-3} D_{Co}$.

Fisher and Tannhauser [24] and Carter and Richardson [25,26] studied the parabolic oxidation kinetics and the self-diffusion of cobalt in CoO as a function of temperature and oxygen pressure. Diffusion data found from tracer

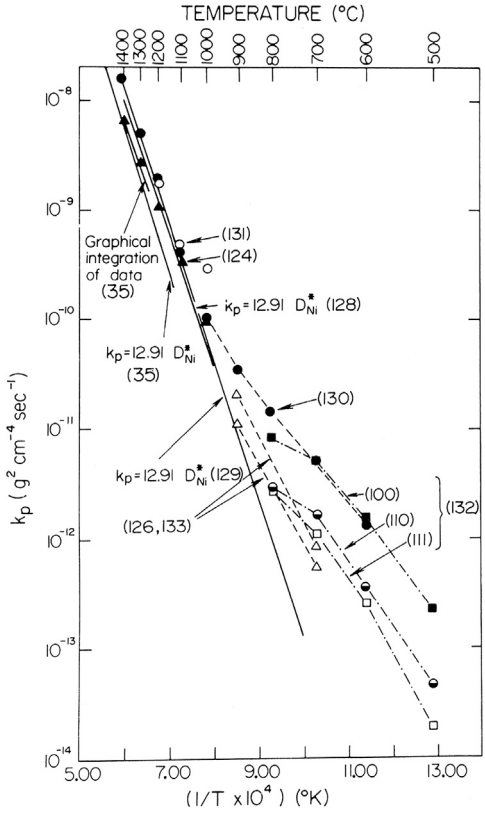

FIGURE 3.7 Parabolic rate constant for NiO scale growth: continuous lines calculated from diffusion data: individual points are measured values. *Reprinted from W.W. Smeltzer, D.J. Young, Prog. Solid State Chem. 10 (1975) 17, with permission from Elsevier.*

experiments are shown in Fig. 3.8. The value of D is proportional to a constant power of p_{O_2} at each temperature, but the power changes with temperature from 0.27 to 0.35 in the range investigated. Assuming, therefore, that the ionisation of cobalt vacancies varied with temperature, the authors wrote

$$\frac{1}{2}O_2 = O_O^{\times} + V_{Co}^{m'} + mh^{\cdot} \qquad [3.72]$$

If the charge balance can be approximated as

$$m\left[V_{Co}^{m'}\right] = [h^{\cdot}] \qquad [3.73]$$

then

$$m^m\left[V_{Co}^{m'}\right]^{m+1} = Kp_{O_2}^{\frac{1}{2}} \qquad [3.74]$$

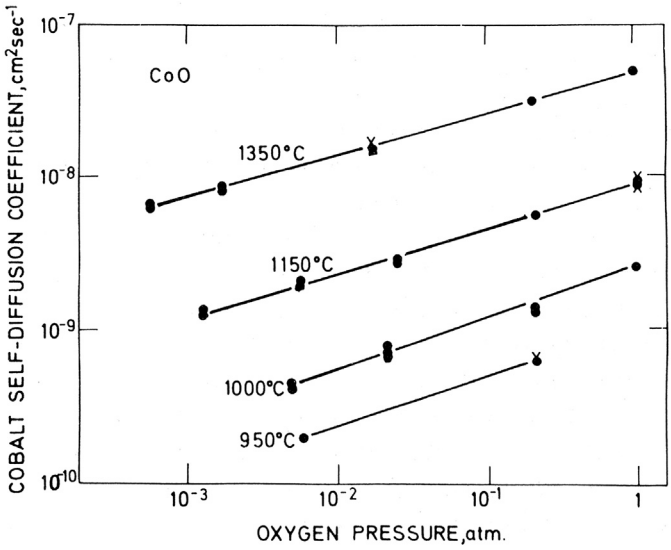

FIGURE 3.8 Tracer diffusion coefficient of cobalt in CoO. *With permission from R.E. Carter, F.D. Richardson, Trans. AIME 200 (1954) 1244; R.E. Carter, F.D. Richardson, Trans. AIME 203 (1955) 336, TMS.*

K being, in this instance, the equilibrium constant for Eq. [3.72]. To ease the integration of Eq. [3.62], which lies ahead, it is expedient at this point to take the logarithmic differential of Eq. [3.74] with $C_v = \left[V_{\mathrm{Co}}^{m'}\right]$

$$\frac{d \ln p_{\mathrm{O}_2}}{d \ln C_v} = 2(m+1) \qquad [3.75]$$

Eq. [3.63] then integrates immediately to yield

$$k_{\mathrm{p}} = (m+1) D_{\mathrm{Co}}^{\mathrm{o}} \left\{ \left(p''_{\mathrm{O}_2}\right)^{1/2(m+1)} - \left(p'_{\mathrm{O}_2}\right)^{1/2(m+1)} \right\} \qquad [3.76]$$

where $D_{\mathrm{Co}}^{\mathrm{o}}$ is the diffusion coefficient at $p_{\mathrm{O}_2} = 1$ atm. The experimental and calculated values were in approximate agreement, as shown in Table 3.3. A more extensive examination of CoO scale growth kinetic measurements has been provided by Kofstad [27], who concluded that the Wagner model describes high temperature ($T > 900°\mathrm{C}$) cobalt oxidation well, with $m \approx 1$.

A disadvantage of the integration procedure leading to Eqs [3.71] and [3.76] is the treatment of n (or m) as a constant, whereas in general it varies as the relative concentrations of V'_m and V''_m change. The difficulty was dealt with by Fueki and Wagner [28] by expressing Eq. [3.62] in differential form

$$D_{\mathrm{Co}} = \frac{|z_{\mathrm{o}}|}{z_{\mathrm{Co}}} \frac{dk_{\mathrm{p}}}{d \ln a_{\mathrm{o}}} \qquad [3.77]$$

This equation was used by Mrowec et al. [29,30] in a careful study of cobalt oxidation kinetics. Values of D_{Co} found from the application of Eq. [3.77] to rate data were in good agreement with directly measured values [26,31].

TABLE 3.3 Measured and Calculated Parabolic Oxidation Rate Constants for Cobalt to Cobaltous Oxide

Pressure: 1 atm	k_w (g cm^{-2} s$^{-1/2}$)		
T/°C	Experimental	Calculated	k_p(exptl)/k_p(calcd)
1000	1.56×10^{-4}	1.65×10^{-4}	0.90
1148	3.05×10^{-4}	3.35×10^{-4}	0.88
1350	8.85×10^{-4}	8.26×10^{-4}	1.16

Gesmundo and Viani [32] considered further the variation of m with oxygen activity and hence with position in the scale. They achieved a better description of the oxygen partial pressure dependence of the rate constant by replacing the right hand side of Eq. [3.62] with the sum of two such terms, one for vacancies and one for interstitials. The latter are more significant at low oxygen potentials, near the oxide-cobalt interface.

3.7.3 Oxidation of Iron

At temperatures above 570°C, iron can form three oxides: wüstite, magnetite and hematite. The Fe-O phase diagram and Arrhenius plots for diffusion in the various phases are shown in Figs 2.2 and 3.9. As already seen (Section 2.2) the iron-oxygen diffusion couple resulting from high-temperature oxidation develops a scale consisting of inner, intermediate and outer layers of wüstite, magnetite and hematite, respectively. The thickness of the wüstite layer would be predicted to be much greater than the others, because the phase field and iron diffusion coefficients for FeO are orders of magnitude larger than for the higher oxides, if the reaction is controlled by solid-state diffusion with local equilibria established at phase interfaces.

Scaling kinetics determined by Paidassi [1] are shown in Fig. 3.10 to be parabolic after a brief initial period of nonsteady-state reaction, indicating diffusion control. The relative thicknesses of the different oxide layers quickly attain steady values, as expected for diffusion controlled oxidation. Furthermore, their values (Fig. 3.11) display the expected relative magnitudes.

It is clear from the Fe-O phase diagram that the approximation $\delta \ll 1$ is inapplicable, and the simplified integral Eq. [3.63] should not be employed. Himmel et al. [35] used the radioactive tracer technique to measure D_{Fe} in wüstite, obtaining the results shown in Fig. 3.12. As would be expected from Eq. [3.58], D_{Fe} increases with departure from stoichiometry. These data were used, together with information on the variation in composition (effectively, δ) with oxygen activity to carry out a graphical integration of Eq. [3.57] for growth of the wüstite scale layer in the temperature range 800−1000°C, at $p_{O_2} = 1$ atm. As seen in Table 3.4, agreement with experiment is good. Similar agreement is found [36] at low oxygen partial pressure.

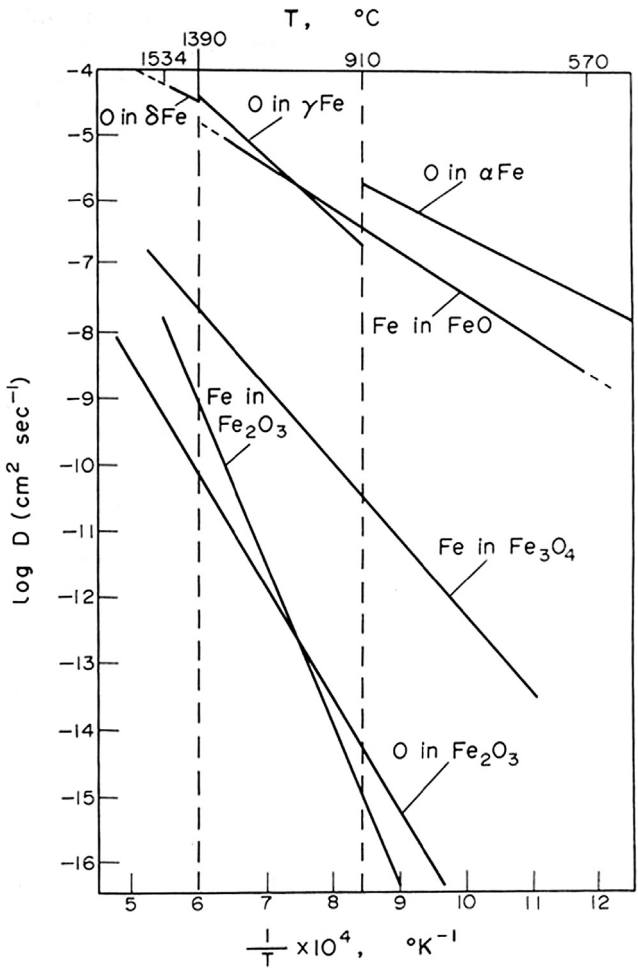

FIGURE 3.9 Iron and oxygen self-diffusion coefficients in iron and iron oxides. *O in Fe (J.H. Swisher, E.T. Turkdogan, Trans. AIME 239 (1967) 426), Fe in FeO (L. Himmel, R.F. Mehl, C.E. Birchenall, Trans. AIME 197 (1953) 827), Fe in Fe_3O_4 (S.M. Klotsman, A.N. Timobeyev, I. Sh, Traktenberg. Phys. Met. Metall. 10 (1960) 93), Fe (R. Lundner, Arkiv Kemi 4 (1952) 381), and O (W.C. Hagel, Trans. AIME 236 (1966) 179) in Fe_2O_3. Reprinted from W.W. Smeltzer, D.J. Young, Prog. Solid State Chem. 10 (1975) 17, with permission from Elsevier.*

A simplified analysis has been provided by Smeltzer [40] and is perhaps more transparent. Assuming that the only defects in $Fe_{1-\delta}O$ are divalent cation vacancies and equivalent concentrations of positive holes, and approximating Fick's first law by a linear vacancy concentration gradient, he obtained

$$J = D_V\left[C_V'' - C_V'\right]/X \qquad [3.78]$$

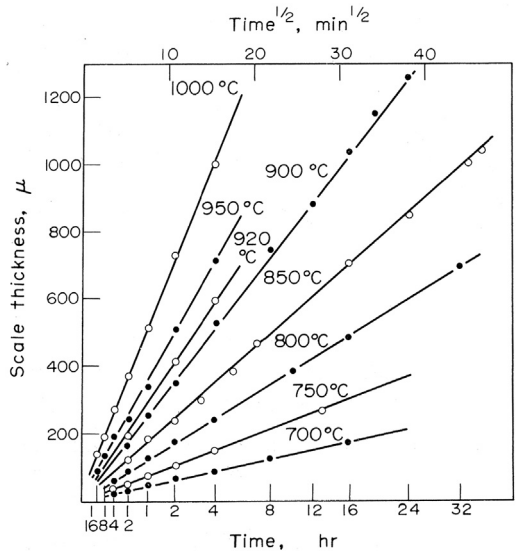

FIGURE 3.10 Parabolic plots for isothermal scaling of iron in air. *Reprinted from J. Paidassi, Rev. Met. 54 (1957) 569, with permission from La Revue de Metallurgie.*

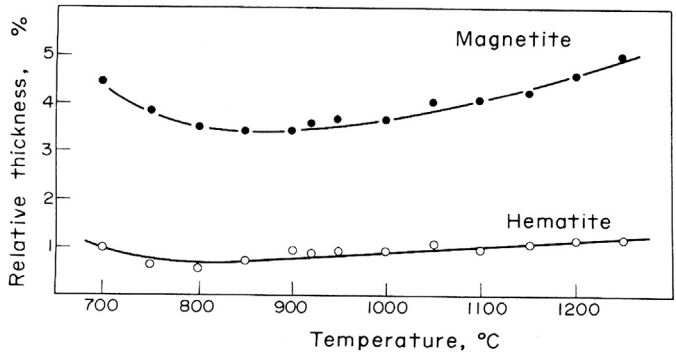

FIGURE 3.11 Relative amounts of iron oxides in scales grown in air. *Reprinted from J. Paidassi, Rev. Met. 54 (1957) 569, with permission from La Revue de Metallurgie.*

and therefore

$$k_p = V_{Fe} D_V \left[C_V'' - C_V' \right] \qquad [3.79]$$

Values for D_V were obtained from the tracer diffusion data for iron in wüstite, using Eq. [3.58]. Estimates of $C_V(X)$ were available from Engell [41], who coulometrically titrated the positive holes as a function of thickness in scales quenched from reaction temperature by equating $C_V'' = \frac{1}{2} C_h$. Rate constants

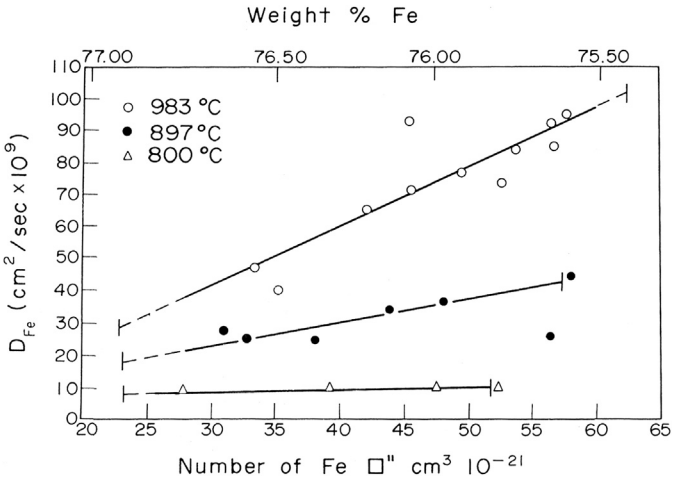

FIGURE 3.12 Iron tracer diffusion coefficient in wüstite. *With kind permission from L. Himmel, R.F. Mehl, C.E. Birchenall, Trans. AIME 197 (1953) 827, Springer Science and Business Media.*

TABLE 3.4 Measured and Calculated Parabolic Oxidation Rate Constants for Iron To Wüstite

Pressure: 1 atm	k_w (g cm^{-2} $s^{-1/2}$)		
T/°C	Experimental	Calculated	k_w(expt)/k_w(calc)
800	2.3×10^{-4}	2.3×10^{-4}	1.0
897	5.0×10^{-4}	4.8×10^{-4}	1.04
983	8.2×10^{-4}	7.7×10^{-4}	1.07

calculated from Eq. [3.79] are compared with experimental results in Fig. 3.13, where good agreement over a wide temperature range is evident.

The apparent success of Eq. [3.79] and the implied validity of its assumption of diffusion via individual, doubly charged vacancies in wüstite are illusory. In Fig. 3.14, the measured nonstoichiometry of wüstite is shown as a function of oxygen potential at a number of temperatures. If the degree of nonstoichiometry were in fact equivalent to the vacancy concentration, and the defects exhibited ideal or Henrian solution behaviour, then a log−log plot such as those of Fig. 3.15 would be a straight line of slope 1/6 or 1/4 for doubly or singly charged vacancies. The real plots are curved, showing that the assumed basis for Eq. [3.79] is a rather crude approximation. This failure is to be expected for the large vacancy concentrations present in wüstite, where vacancy interactions such as cluster formation [45,46] should be taken into account.

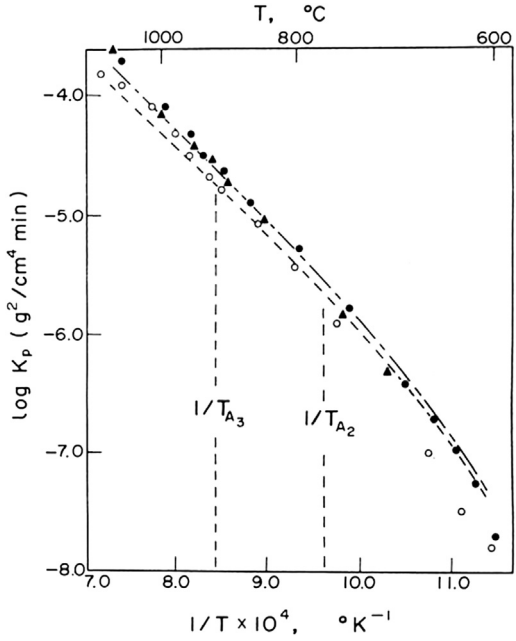

FIGURE 3.13 Calculated (curves) parabolic rate constants for wüstite growth on iron compared with measured values [41—43]. *Reprinted with permission from W.W. Smeltzer, Acta Met. 8 (1960) 377, Elsevier.*

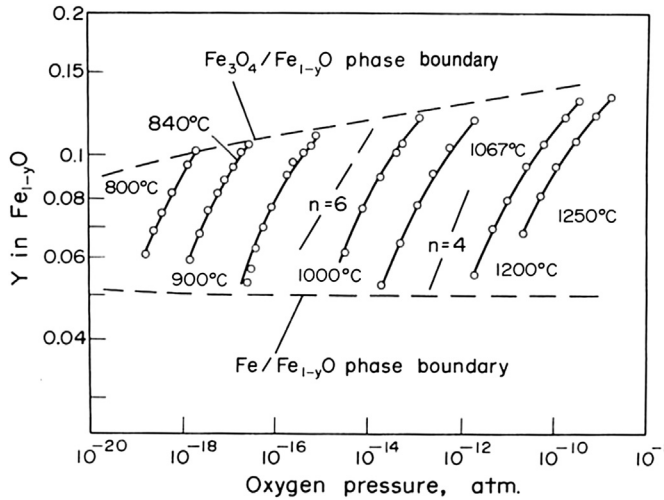

FIGURE 3.14 Nonstoichiometry of wüstite at several temperatures. *Reprinted from P. Kofstad, A.Z. Hed, J. Electrochem. Soc. 115 (1968) 102, by permission of The Electrochemical Society and P. Vallet, P. Raccah, Mem. Sci. Rev. Met. 62 (1965) 1, published with permission from La Revue de Metallurgie.*

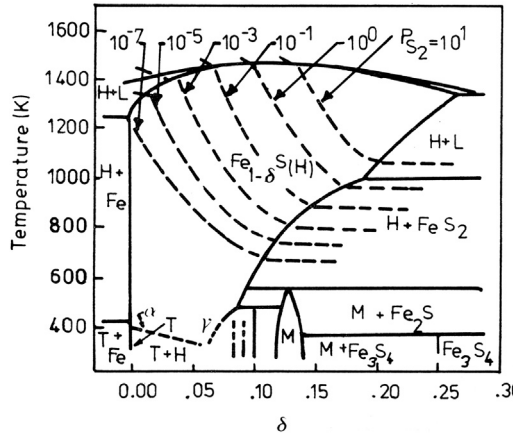

FIGURE 3.15 Phase diagram for Fe-S in the $Fe_{1-\delta}S$ region with equilibrium sulphur partial pressure isobars in kPa.

The diffusion coefficient used in Eq. [3.79] is some sort of average, representing the participating species. It must therefore be concluded that although it provides an empirically successful means of predicting the growth of wüstite, the model provides only limited insight into the defect nature of this oxide or its diffusion mechanism.

3.7.4 Sulphidation of Iron

The iron sulphidation reaction has been studied intensively as a test case for the applicability of Wagner's theory. A review [47] of the work serves also to illustrate the considerable differences between oxidation and sulphidation reactions.

The Fe-S phase diagram in the $Fe_{1-\delta}S$ region is shown in Fig. 3.15. As seen, the nonstoichiometry is a strong function of temperature and p_{S_2} and can range up to about 25 atom percent. The material is always metal deficit with the principal defects being metal vacancies.

Usually a much larger degree of nonstoichiometry is found in sulphides than in the analogous oxides. Factors which contribute to this are the larger anion size and lower lattice energy of the sulphides. Thus point defects are more easily created and deviation from stoichiometry thereby arrived at. What is important from the point of view of metal sulphidation is that a material containing a high density of lattice defects will evidence a high diffusion rate and therefore form only a poorly protective scale.

At temperatures below that of the Fe−S eutectic, pure iron sulphidises to form, in the relatively short-term, a compact, tightly adherent scale. When the value of p_{S_2} is sufficiently high (see Fig. 3.15) the scale consists of a thin

surface layer of FeS_2 over a thick layer of $Fe_{1-\delta}S$, but at lower values of p_{S_2}, only the monosulphide phase is formed. Since the rate of formation of FeS_2 is orders of magnitude less than for $Fe_{1-\delta}S$, attention is focused on the monosulphide formation reaction.

The compact monosulphide scale grows according to parabolic kinetics, suggesting that the process is controlled by solid-state diffusion. Since the electron conduction characteristics of $Fe_{1-\delta}S$ are metallic in nature and since the self-diffusion coefficient of sulphur, D_S, is much less than that of iron, D_{Fe}, then Wagner's theory predicts that the flux of iron supports sulphide scale growth rate

$$k_p = \int_{a'_s}^{a''_s} D_{Fe} \frac{1}{1-\delta} d \ln a_s \qquad [3.80]$$

The variation of the tracer diffusion coefficient of iron with stoichiometry has been measured by Condit et al. [48] in single crystal $Fe_{1-\delta}S$ as

$$D_{Fe} = D_o \delta \exp[-Q/RT] \qquad [3.81a]$$

with

$$Q = 81 + 84\delta \text{ kJ mol}^{-1} \qquad [3.81b]$$

where D_o has the values 1.7×10^{-2} and 3.0×10^{-2} cm^2 s^{-1} for diffusion in the a- and c-directions, respectively. The way in which δ varies with T and p_{S_2} was determined by Toulmin and Barton [49], permitting the numerical integration of Eq. [3.80]. Fryt et al. [50,51] found very good agreement between rates calculated in this way and measured values over wide ranges of temperature (600–980°C) and p_{S_2} (5×10^{-11} to 2×10^{-2} atm).

A comparison of $Fe_{1-\delta}O$ and $Fe_{1-\delta}S$ scaling rates is informative. At a temperature of 800°C, a wüstite layer grows at 1×10^{-8} cm^2 s^{-1}, whereas $Fe_{1-\delta}S$ grows at 1×10^{-5} cm^2 s^{-1} when $P_{S_2} = 0.01$ atm. The value of δ (measured by chemical analysis) at the $Fe_{1-\delta}O/Fe_3O_4$ interface is ~ 0.1, and at the $Fe_{1-\delta}S$ scale-gas interface ~ 0.12. Thus the reason for the large difference in rates lies in the diffusion coefficients rather than the degree of nonstoichiometry. In wüstite at 800°C, $D_{Fe} = 10^{-7}$ cm^2 s^{-1}, whereas in $Fe_{1-\delta}S$, it is $\sim 10^{-5}$ cm^2 s^{-1}. These differences reflect the different crystal structures ($Fe_{1-\delta}S$ has the hexagonal NiAs structure rather than the cubic NaCl structure of $Fe_{1-\delta}O$) and lattice spacing of the two iron compounds.

3.7.5 Effects of Oxidant Partial Pressure on the Parabolic Rate Constant

Wagner's treatment of diffusion controlled scale growth explicitly recognises the effect of oxidant partial pressure by relating the flux of diffusing species to

chemical potential gradients in the scale. Local equilibrium at the metal-scale interface for the case of negligible deviation from stoichiometry may be written

$$\mathrm{M} + \frac{1}{2}\mathrm{O_2} = \mathrm{MO}$$

$$a'_m a'_{\mathrm{o}} = 1/K \qquad [3.82]$$

and fixes $a'_m = 1$ and $a'_{\mathrm{o}} = 1/K$. Changing the ambient gas cannot change these values. However, at the scale-gas interface, the oxidant partial pressure can be varied, and then

$$a''_m = 1 \Big/ K p_{\mathrm{O_2}}^{\frac{1}{2}} \qquad [3.83]$$

Thus the gradients in both metal and oxidant activity are affected by changes in the ambient atmosphere, as are the diffusive fluxes within the scale.

For a metal deficit oxide such as $\mathrm{Fe}_{1-\delta}\mathrm{O}$, CoO or NiO, Eq. [3.63] applies if deviations from stoichiometry can be ignored. If, furthermore, $D_V \neq f(a_{\mathrm{o}})$, the integral is evaluated using the point defect equilibrium Eq. [3.72] to provide the change of variable given by Eq. [3.75], resulting in Eq. [3.76]. Because $p''_{\mathrm{O_2}}$ is usually orders of magnitude greater than the scale-gas equilibrium value $p'_{\mathrm{O_2}}$, we can write

$$k_{\mathrm{p}} = (m+1) D^{\mathrm{o}}_{\mathrm{M}} p_{\mathrm{O_2}}^{\frac{1}{2(m+1)}} \qquad [3.84]$$

where $D^{\mathrm{o}}_{\mathrm{M}}$ is the metal diffusion coefficient at $p_{\mathrm{O_2}} = 1$ atm.

Fueki and Wagner [28] tested the applicability of Eq. [3.84] to the oxidation of nickel and found m to vary from 2 at 1000°C to 0.75 at 1400°C. They concluded on this basis that doubly charged vacancies, as identified in Eq. [3.72], were predominant at 1000°C, but singly charged vacancies became more important at higher temperatures.

The effect of $p_{\mathrm{O_2}}$ on k_{p} for cobalt oxidation is shown in Fig. 3.4. At lower $p_{\mathrm{O_2}}$ values, only CoO is formed, and Eq. [3.84] describes the variation in k_{p} with oxidant activity well, with $m \approx 1$. When an outer layer of $\mathrm{Co_3O_4}$ is formed at higher oxygen activities, it is rather thin, and the measured total weight gain corresponds essentially to CoO layer growth. As seen in Fig. 3.3, the rate does not vary with $p_{\mathrm{O_2}}$ in this regime. This is a consequence of the fact that the boundary value of a_{o} at the CoO outer interface is set by the equilibrium

$$3\mathrm{CoO} + \frac{1}{2}\mathrm{O_2} = \mathrm{Co_3O_4} \qquad [3.85]$$

and is therefore unaffected by changes to the gas atmosphere.

A more detailed study of the effect of $p_{\mathrm{O_2}}$ on CoO scale growth was undertaken by Mrowec and Przybylski [30] who showed that $2(m+1)$ varied

from 3.4 at 950°C to 3.96 at 1300°C. They attributed the deviation from the value 4 expected for singly charged vacancies to a contribution from intrinsic Frenkel defects. However, when much lower p_{O_2} values were investigated [24], the defect properties of CoO were found not to conform with the continuous power relationship of Eq. [3.75].

Studying the p_{O_2} dependence of wüstite layer growth is difficult because the oxygen partial pressures required are so low. At 1000°C, Fe_3O_4 forms on top of the wüstite layer at $p_{O_2} = 10^{-12}$ atm. As seen earlier (Fig. 3.11), wüstite continues to constitute the majority of the scale, and measured reaction rates correspond essentially to that of $Fe_{1-\delta}O$ layer growth. Since the boundary values of oxygen activity at the metal scale and $Fe_{1-\delta}O/Fe_3O_4$ interfaces are fixed by the phase equilibria at these surfaces, the diffusive flux supporting wüstite layer growth is independent of the ambient p_{O_2} value. The low p_{O_2} values necessary to grow $Fe_{1-\delta}O$ alone can be achieved using CO/CO_2 or H_2/H_2O atmospheres. Pettit and Wagner [52] and Turkdogan et al. [53] have oxidised iron in such atmospheres and have found the reactions to be controlled initially by surface processes involving CO_2 or H_2O. Eventually parabolic kinetics take over, at the rates predicted from Wagner's theory.

Growth rates of metal excess, n-type oxides show interesting oxidant pressure effects. Considering the formation of interstitial cations (eg, in $Zn_{1+\delta}O$)

$$MO = M_i^{m\bullet} + me' + \frac{1}{2}O_2(g) \qquad [3.86]$$

If the charge balance can be written

$$C_e = mC_{M_i} \qquad [3.87]$$

then

$$C_{M_i} = \left(\frac{K}{m}\right)^{1/(m+1)} p_{O_2}^{-1/2(m+1)} \qquad [3.88]$$

where K is the equilibrium constant for Eq. [3.86]. As expected, adding more oxygen to a metal excess oxide reduces the deviation from stoichiometry.

Logarithmic differentiation then yields

$$\frac{d \ln p_{O_2}}{d \ln C_{M_i}} = -2(m+1) \qquad [3.89]$$

and integration of Wagner's rate expression leads to

$$k_p = (m+1)D_{M_i}\left\{\left(p'_{O_2}\right)^{-1/2(m+1)} - \left(p''_{O_2}\right)^{-1/2(m+1)}\right\} \qquad [3.90]$$

In the usual case where $p''_{O_2} \gg p'_{O_2}$, the negative exponent makes the second term in the braces much less than the first, and

$$k_p = (m+1)D_{M_i}\left(p'_{O_2}\right)^{-1/2(m+1)} \qquad [3.91]$$

Since p'_{O_2} is established by the metal-oxide equilibrium at the base of the scale, it is independent of the gas composition. Thus the rate of growth of a metal excess oxide is usually independent of p_{O_2}. A similar argument can be developed for metal deficit oxides in which anion vacancies are the principal defects [27].

The correctness of this prediction for the growth of $Zn_{1+\delta}O$ was demonstrated by Wagner and Grunewald [54], who obtained essentially the same oxidation rate at oxygen partial pressures of 1 and 0.02 atm and a temperature of 390°C.

The rate at which iron sulphidises varies in a complex manner with p_{S_2} [50,51]. This is a consequence of vacancy interactions at the high concentrations involved, and Wagner's kinetic analysis cannot be used to provide insight into the defect properties of $Fe_{1-\delta}S$

3.7.6 Effect of Temperature on the Parabolic Rate Constant

The rate constant for growth of a metal deficit oxide given by Wagner's theory Eq. [3.61] is dependent on temperature in three ways. The diffusion coefficient is thermally activated, $D_M = D_O \exp(-Q/RT)$. The boundary value of the oxygen activity a'_o, which is one of the limits of integration, is set by the temperature-dependent, metal-oxide equilibrium Eq. [3.82], whence, through Eq. [2.28]:

$$a'_o = \exp\left(\frac{+\Delta H^\circ(\mathrm{MO})}{RT}\right)\exp\left(\frac{-\Delta S^\circ(\mathrm{MO})}{R}\right) \qquad [3.92]$$

Finally, the functional relationship between nonstoichiometry and a'_o is itself temperature-dependent through the temperature effect on intrinsic disorder Eq. [3.18]. This last effect is significant if the degree of nonstoichiometry is large and must be dealt with by numerical integration, as has been done for $Fe_{1-\delta}O$ [35] and $Fe_{1-\delta}S$ [47]. Usually, however, it is ignored.

The importance of the temperature effect on a'_o depends on the nature of the oxide. For a metal deficit oxide, we have seen that the integrated form Eq. [3.76] can be simplified on the basis $a''_o \gg a'_o$ to the form Eq. [3.84]. Thus the temperature dependence of a'_o is unimportant. The activation energy for the scaling rate constant is in this case the same as that of the metal diffusion coefficient.

A different conclusion is reached for metal excess oxide, where the defect concentration is inversely proportional to some power of p_{O_2}. In the usual situation where $a''_o > a'_o$, it follows that

$$\frac{1}{a_o'} \gg \frac{1}{a_o''} \qquad [3.93]$$

and the integrated form of the rate expression is given by Eq. [3.91]. Rewriting this to show the temperature effect explicitly, we obtain

$$k_p = (m+1)D_o \exp\left(-\frac{Q}{RT}\right)\exp\left\{\frac{-\Delta H^\circ(\mathrm{MO})}{(m+1)RT}\right\}\exp\left\{\frac{\Delta S^\circ(\mathrm{MO})}{(m+1)R}\right\} \qquad [3.94]$$

thus observing that the activation energy for k_p is given by $\left[Q + \Delta H^\circ(\mathrm{MO})/(m+1)\right]$.

In the foregoing discussion of temperature effects, we have assumed that the scale was a single phase and that its outer surface was in contact with gas at some fixed value of $a_o'' = p_{O_2}^{\frac{1}{2}}$. However, if an additional layer develops, as in the cases of iron and cobalt (Fig. 3.1), then a_o'' is set by the interfacial equilibrium between the two oxides, as expressed, eg, by Eq. [3.85]. The temperature effect on the rate of CoO growth is then found from Eq. [3.76] as

$$k_p = (m+1)D_O \exp(-Q/RT)\exp\left[+\Delta H^\circ/(m+1)RT\right]\exp\left[-\Delta S^\circ/(m+1)R\right] \qquad [3.95]$$

where ΔH°, ΔS° refer to the $CoO \rightarrow Co_3O_4$ reaction in Eq. [3.85]. Kofstad's compilation [27] of cobalt oxidation rate data is reproduced in Fig. 3.16.

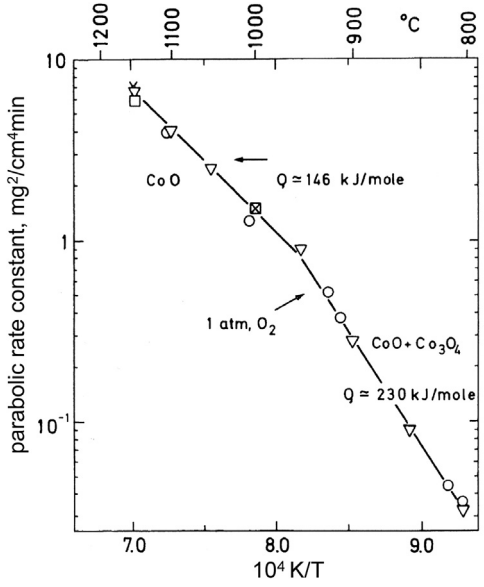

FIGURE 3.16 Temperature effects on cobalt oxidation rates in 1 atm O_2. *Reprinted from P. Kofstad, High Temperature Corrosion, Elsevier Applied Science, London, (1988), with permission from Elsevier.*

At high temperatures, where only CoO is formed, the activation energy is equal to that of D_{Co} at 160 kJ mol^{-1}. At lower temperatures, a thin layer of Co_3O_4 forms on top of the CoO, but the measured overall oxidation rate corresponds closely to the growth of the majority CoO layer and is given to a good approximation by Eq. [3.95]. Taking $\Delta H°(3.85) = 183$ kJ mol^{-1}, the activation energy for scaling is then predicted to be $160 + 183/2 = 252$ kJ mol^{-1}. This is in reasonable agreement with the experimental finding of 230 kJ mol^{-1}. The rate of CoO growth is 'decreased' at lower temperatures because a''_o, as established by the CoO/Co_3O_4 equilibrium, is much lower than the gas-phase value of 1 atm.

3.7.7 Other Systems

Wagner's theory has been shown to be successful in describing the oxidation of copper to form metal deficit Cu_2O. This first demonstration is of historic interest, as it was performed by Wagner himself [54]. It is also unusual in that the transport properties of Cu_2O were measured electrochemically. Later results on copper oxidation have been reviewed [27,33] and are considered to indicate that the defect nature of Cu_2O is more complex than the neutral vacancy model

$$\frac{1}{2}O_2(g) = 2V^X_{Cu} + O^X_O \qquad [3.96]$$

deduced by Wagner.

The high temperature oxidation of silicon is important in solid-state device technology, and it has accordingly been studied intensively. The reaction product is amorphous or glassy SiO_2, which is highly protective. The early kinetic investigations of Deal and Grove [55] led to the parabolic-linear rate equation

$$X^2 + AX = k_p(t + \tau) \qquad [3.97]$$

for a reaction in dry oxygen. Here k_p/A is a linear rate constant related to phase boundary reactions, and τ is a correction to allow for the non-zero oxide film thickness at the commencement of the reaction. The magnitude and activation energy of k_p were shown [55,56] to agree with those of oxygen diffusion through glassy silica.

The Wagner equation for oxygen diffusion control is simply

$$k_p = \int_{p'_{O_2}}^{p''_O} D_o d \ln p_{O_2} \qquad [3.98]$$

and for D_o independent of oxygen activity, this integrates to yield

$$k_p = D_o\left[p''_{O_2} - p'_{O_2}\right] \approx D_o p''_{O_2} \quad [3.99]$$

thus accounting for the original observation [55] that $k_p \propto p_{O_2}$ and indicating that the diffusing species are oxygen molecules.

Very different results are obtained at high temperatures and low p_{O_2} values, because volatilisation of SiO(g) becomes important. This situation is discussed in Section 3.10.

A few other systems have been used to test the validity of the Wagner approach: silver sulphidation and bromination, as well as CuI formation. Scaling rates were found to be in good order of magnitude agreement with predictions based on the transport properties of the relevant compounds [57–59].

3.7.8 Utility of Wagner's Theory

Wagner's equations express succinctly the parameters affecting oxidation rates: the material properties of the oxide, oxidant partial pressure and temperature. Consider the relative rates at which $Fe_{1-\delta}O$, CoO and NiO grow at 1000°C (Table 3.1). All three oxides have the same crystal structure and contain cation vacancies. To a first approximation, we ignore differences in atomic weights, lattice spacing and, most importantly, defect interactions and suppose that D_V has the same value in each oxide. This approximation can be tested, using $D_M = D_V C_V$ on the assumption of uncorrelated diffusion and measured values of D and $\delta = C_V$. As seen in Table 3.5, D_V values calculated in this way are in fact within an order of magnitude. To this degree of approximation then, the differences in metal self-diffusion coefficient can be attributed directly to oxide nonstoichiometry. Recalling that for metal deficit oxides,

$$k_p = (m+1)D^o_M p^{1/2(m+1)}_{O_2} \quad [3.84]$$

then at $p_{O_2} = 1$ atm, k_p is 1, 2 or 3 times D^o_M for vacancy charges of 0, 1 or 2, respectively. The rate data for cobalt and nickel at 1000°C and $p_{O_2} = 1$ atm in

TABLE 3.5 Comparative Data for Metal Deficit Oxides at 1000°C

Oxide	Measured Data			Calculated D_v ($cm^2\ s^{-1}$)
	k_p ($cm^2\ s^{-1}$)	D_M ($cm^2\ s^{-1}$)	C_v (Fraction)	
$Fe_{1-\delta}O$	2×10^{-7}	8×10^{-7}	0.13	6.2×10^{-6}
CoO	3.3×10^{-9}	1.2×10^{-9}	0.01	1.2×10^{-7}
NiO	9×10^{-11}	1×10^{-11}	10^{-5}	1×10^{-6}

Table 3.5 are in reasonable accord with this prediction for $m = 2$. In the case of iron, p_{O_2} has the value set by the FeO/Fe_3O_4 equilibrium and, for $m = 2$, the value of k_p predicted from Eq. [3.84] is $2 \times 10^{-8}\,cm^2\,s^{-1}$, an order of magnitude lower than the measured quantity. Nonetheless, the widely different growth rates of these three oxide scales can be understood, and semi-quantitatively predicted, simply from a knowledge of their nonstoichiometry.

It was the achievement of Wagner and the other early investigators in Germany to recognise that nonstoichiometry corresponded to the existence of lattice defects, and that furthermore, these defects provided the mechanism of diffusion and scale growth. Wagner's theory has been shown to be quantitatively successful in a convincing number of cases. A principal reason for the limited utility of the theory is the lack of sufficient data to permit the accurate integration of rate equations like Eq. [3.61]. From a practical point of view, it is easier to measure a parabolic rate constant than to predict it by determining diffusion coefficients and deviations from stoichiometry as functions of oxygen activity. The real value of the theory is in providing a fundamental understanding of the oxidation mechanism. As we have seen, the thermodynamic and diffusional analysis leads to an understanding of and the ability to predict the effects of temperature and oxidant partial pressure.

Despite the intellectually satisfying nature of the Wagner analysis, it is prudent to bear in mind its limitations. As we have seen, the theory works well for a moderately nonstoichiometric oxide like CoO but fails to reveal the complexities of diffusion in highly disordered solids like $Fe_{1-\delta}O$ and $Fe_{1-\delta}S$. More seriously, it cannot be used to predict the growth rates of slow growing (and therefore important) oxides like Cr_2O_3 and Al_2O_3. These oxides have immeasurably small deviations from stoichiometry, and their diffusion properties are not well understood. These difficulties result from the nature of the oxides. Firstly, the native lattice defect concentrations are so small that even low concentrations of impurities can dominate the oxide. Secondly, and for the same reason, diffusion via pathways other than the oxide lattice are usually important. We now consider these effects.

3.8 IMPURITY EFFECTS ON LATTICE DIFFUSION

In reality metals are seldom anywhere near pure. Even so-called 'high purity' metals usually contain impurities at concentrations in the parts per million (ppm) range. One exception to this generalisation might be silicon, which is routinely zone-refined to very high purity levels, in order to avoid unwanted dopants which would affect semiconductor properties. The presence of impurity ions of valence different from that of the solvent species can change the defect concentration through their effect on charge balance. Consider the substitutional dissolution of chromium in NiO:

$$2Cr + 3\left(Ni_{Ni}^{\times} + O_O^{\times}\right) = 2Cr_{Ni}^{\bullet} + V_{Ni}'' + 3O_O^{\times} + 3Ni \qquad [3.100]$$

or, equivalently

$$Cr_2O_3(+NiO) = 2Cr_{Ni}^{\bullet} + V_{Ni}'' + 3O_O^{\times}(+NiO) \quad [3.101]$$

The different effective charge of the impurity, or dopant, is seen to be accommodated by an adjustment in the number of cation vacancies.

In the first formulation, chromium metal is oxidised by NiO, displacing nickel metal, as would be predicted from the relative stabilities of Cr_2O_3 and NiO. In the second formulation, the NiO lattice is extended by the dissolution of some chromia. In writing these equations, it is assumed that chromium is dissolved substitutionally onto the normal cation sublattice. Moreover, the cation to anion site ratio of the solvent oxide is maintained, as its crystallography is unchanged. To formulate the equations it is necessary, of course, to know the natural defect type of the solvent oxide.

Consider now the cation vacancy concentration when the doped oxide is at equilibrium with a gas. In addition to Eq. [3.101], we have

$$\frac{1}{2}O_2(g) = O_O^{\times} + V_{Ni}'' + 2h^{\bullet} \quad [3.102]$$

$$C_V C_h^2 = K p_{O_2}^{\frac{1}{2}} \quad [3.103]$$

if only doubly charged vacancies can form. The charge balance is now written

$$2C_V = C_{Cr} + C_h \quad [3.104]$$

and substitution for C_h from Eq. [3.103] then leads to

$$2C_V = C_{Cr} + K^{\frac{1}{2}} p_{O_2}^{\frac{1}{4}} \Big/ C_V^{\frac{1}{2}} \quad [3.105]$$

Thus doping with a higher valent cation has the effect of increasing the vacancy concentration and making it less sensitive to oxygen partial pressure. The effects on k_p are predicted to be qualitatively similar. Nickel containing low concentrations of chromium has been found [60,61] to oxidise faster than pure nickel, in agreement with this prediction. Using similar reasoning, it is found that dissolution of a lower valence cation in a metal deficit oxide decreases the concentration of vacancies, and hence the oxidation rate.

In the case of a metal excess oxide like ZnO, where the ionic defects have a positive charge, the effects of aliovalent doping are reversed. Consider the incorporation of a higher valent cation such as Cr^{3+}

$$Cr_2O_3(+ZnO) = 2Cr_{Zn}^{\bullet} + 2O_o^{\times} + 2e' + \frac{1}{2}O_2(g) \quad [3.106]$$

Because formation of a cation vacancy is energetically unfavourable in an n-type oxide, site balance is instead maintained via the ejection of gaseous

oxygen and the formation of free electrons. If the interstitial zinc species are fully ionised, we have also

$$\mathrm{ZnO} = \mathrm{Zn}_i^{\cdot\cdot} + 2e' + \frac{1}{2}\mathrm{O}_2 \qquad [3.107]$$

$$K = C_{\mathrm{Zn_i}} C_e^2 p_{\mathrm{O}_2}^{\frac{1}{2}} \qquad [3.108]$$

and the charge balance becomes

$$2C_{\mathrm{Zn_i}} + C_{\mathrm{Cr_{Zn}}} = C_e \qquad [3.109]$$

Combination of Eq. [3.108] and [3.109] then yields

$$2C_{\mathrm{Zn_i}} + C_{\mathrm{Cr_{Zn}}} = \frac{K^{\frac{1}{2}}}{C_{\mathrm{Zn_i}}^{\frac{1}{2}} p_{\mathrm{O}_2}^{\frac{1}{4}}} \qquad [3.110]$$

and the addition of chromium is seen to decrease the concentration of zinc interstitials and would therefore be expected to decrease the zinc oxidation rate.

The various combinations of higher or lower valent dopants with stoichiometric oxides (both Schottky and Frenkel type) or nonstoichiometric compounds (metal excess or deficit, lattice or interstitial species) have been considered in detail, as they are important to the study of solid-state chemistry [62]. However, the value of dopant chemistry in understanding or predicting oxidation behaviour is far from clear. Consider even the simple case of chromium doping NiO to the extent where Eq. [3.105] can be approximated as

$$C_V = \frac{1}{2} C_{\mathrm{Cr}} \qquad [3.111]$$

The rate expression Eq. [3.63] then becomes

$$k_{\mathrm{p}} = D_V \int_{a'_{\mathrm{o}}}^{a''_{\mathrm{o}}} C_{\mathrm{Cr}} d \ln a_{\mathrm{o}} \qquad [3.112]$$

and to proceed further, we require knowledge of the chromium concentration profile within the scale. Information of this sort is not available. Moreover, the ideal or Henrian solution (Section 2.3) behaviour implicit in equilibrium concentration relationships like Eq. [3.103] is highly unlikely to apply in the presence of dopants.

3.9 MICROSTRUCTURAL EFFECTS

Wagner's theory assumes the oxide scale to be continuous, coherent, perfectly bonded to the substrate metal and capable of diffusion only via lattice defects. As seen in the preceding sections, these assumptions can be successful,

particularly at high temperatures in systems containing large concentrations of lattice defects. At lower temperatures and in oxides with less defective lattices, they can fail. Nickel oxidation (Fig. 3.7) provides an example of agreement between theory and experiment at high temperatures, but measured rates are much higher than predicted at low temperatures. As is clear from the measurements the activation energy has a smaller value at lower temperatures, and a different mechanism must be in effect. That mechanism has been shown to be grain boundary diffusion.

3.9.1 Grain Boundary Diffusion

Oxide scales are polycrystalline, and grain size can vary considerably. As seen in Fig. 3.1, the NiO grain size in a scale grown at 1100°C is tens of microns. In oxide grown at 800°C, the columnar grains seen in Fig. 3.17 are about 1 μm across. At lower temperatures, the grains are even finer and show evidence of coarsening with time (Fig. 3.18).

Grain boundary diffusion is often more important than lattice diffusion at low temperatures. A principal reason for this is the lower activation energy of the boundary process, corresponding to the more disordered structures in the boundaries [65]. A second reason is the usually finer grain size and hence more numerous boundaries encountered at lower temperatures, as illustrated above for NiO. The additional possibility of impurity species segregation to grain boundaries is considered in Sections 4.4, 7.5 and 11.4.

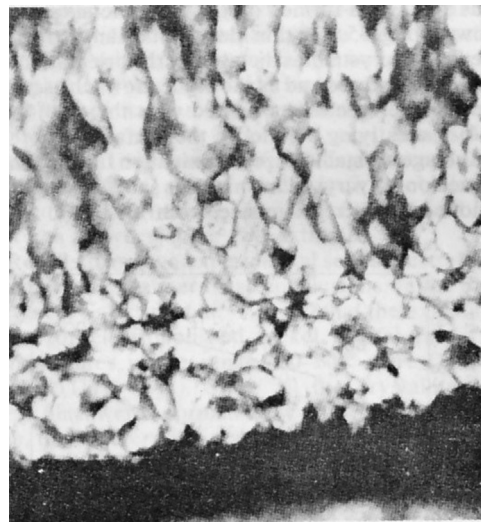

FIGURE 3.17 SEM view of cross-section through NiO scale. *With kind permission from R. Herchl, N.N. Khoi, T. Homma, W.W. Smeltzer, Oxid. Met. 4 (1972), 35, Springer Science and Business Media.*

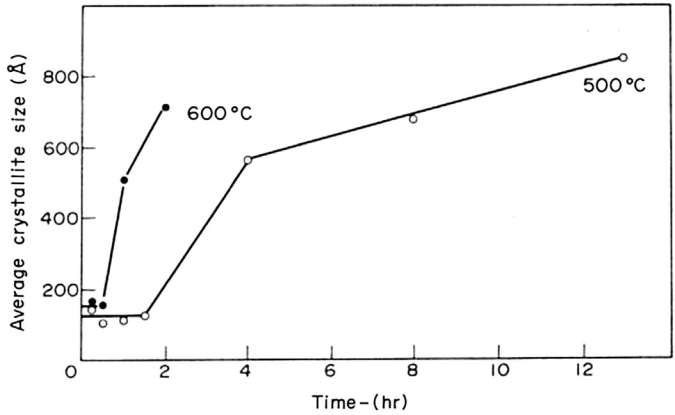

FIGURE 3.18 Average grain size in NiO scales as a function of oxidation time. *Reprinted from J.M. Perrow, W.W. Smeltzer, J.D. Embury, Acta Met. 16 (1968) 1209, with permission from Elsevier.*

A useful way of describing diffusion in a polycrystalline material was proposed by Hart [66] and adapted by Smeltzer et al. [67] to the nickel oxidation case. An effective diffusion coefficient is defined as a weighted sum of lattice and boundary contributions

$$D_{\text{eff}} = D_{\text{L}}(1-f) + D_{\text{B}}f \qquad [3.113]$$

where f is the fraction of diffusion sites within the boundaries, and D_{L}, D_{B} are the self-diffusion coefficients for the bulk lattice and boundaries, respectively. Using the linear approximation to the oxidation rate equation

$$\frac{dX}{dt} = VD_{\text{eff}}\frac{\Delta C}{X} \qquad [3.114]$$

and integrating, one obtains

$$X^2 = 2VD_{\text{L}}\Delta C\int_o^t [1 + (D_{\text{B}}/D_{\text{L}})f]dt \qquad [3.115]$$

so that the effective rate constant for fixed f and predominant boundary diffusion is

$$k_{\text{p}} = V\Delta CD_{\text{B}}f \qquad [3.116]$$

More complex kinetics result if the oxide grain size distribution varies with time [63,64,67]. If grain nucleation and growth depend on instantaneous scaling rate, then grain size will vary with position in the scale, reflecting the time at which the local oxide formed. This situation is discussed in Section 7.2.3. More simply, the scale is regarded as being characterised by an average grain size, which evolves with time.

If the density of rapid diffusion sites decays according to first order kinetics [67]

$$f = f^{\circ} \exp(-kt) \qquad [3.117]$$

then

$$X^2 = 2k_p\left\{t + \frac{f^{\circ} D_B}{kD_L}(1 - e^{-kt})\right\} \qquad [3.118]$$

where f° is the initial value of f. If, on the other hand, the decay in f is due to recrystallisation and grain growth in the oxide [63]

$$f = 2d/D_t; D_t^2 - D_o^2 = Gt \qquad [3.119]$$

and Eq. [3.118] becomes

$$X^2 = 2k_p t\left\{1 + \frac{4D_B d}{D_L G}\left[\frac{(D_o^2 - Gt)^{\frac{1}{2}} - D_o}{t}\right]\right\} \qquad [3.120]$$

Here, the grains are modelled as cubes of edge D_t, which have grown from an original size D_o with a growth constant G, and the boundaries have a width, d. Low temperature nickel single crystal oxidation rates have been successfully described [63] using Eq. [3.120] with a value for k_p calculated for lattice diffusion from Wagner's theory. The success of this procedure can be seen in Fig. 3.19.

The reaction was controlled by boundary diffusion in the temperature range 500−800°C. Assuming $d = 1$ nm and using measured grain sizes, the activation energy was estimated at 130−145 kJ mol^{-1}, compared with 255 kJ mol^{-1} for lattice diffusion of nickel and for k_p. Graham et al. [68] estimated the activation energy for boundary diffusion as 169 kJ mol^{-1}, using first order kinetics Eq. [3.117] for the decrease in boundary density, in approximate agreement.

A review [33] of correlations of oxide microstructures with oxidation rates of several metals confirms that boundary diffusion is an important component of scale growth. Isotope diffusion measurements in growing NiO scales [69] have demonstrated that boundary diffusion is dominant at 500 and 800°C. Atkinson et al. [70,71] used measured values for lattice, dislocation and grain boundary diffusion in the grain growth model Eq. [3.119] and successfully modelled low temperature oxidation rates.

The intensively studied nickel oxidation reaction has been shown conclusively to be dominated by grain boundary diffusion at temperatures below about 900°C. It seems likely that the same will be true for all oxides, in an appropriate temperature regime, and that the lower the value of D_L, then the higher the temperature range in which boundary diffusion will be the

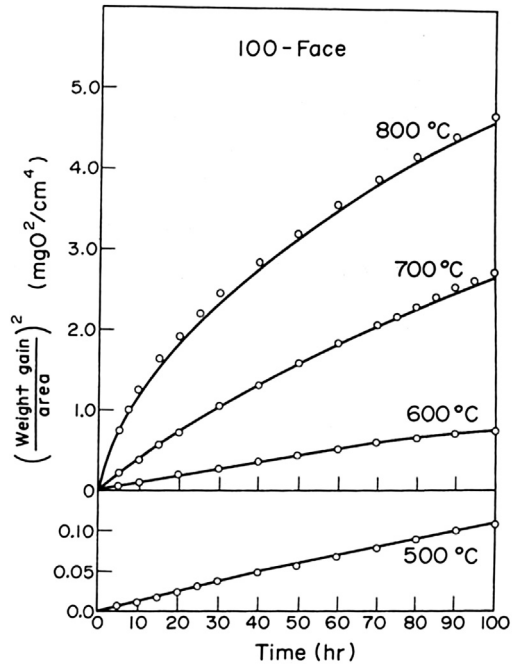

FIGURE 3.19 Experimental results and curves calculated from Eq. [3.120] for the growth of NiO scales on a (100) Ni face. *Reprinted from R. Herchl, N.N. Khoi, T. Homma, W.W. Smeltzer, Oxid. Met. 4 (1972), 35, with kind permission from Springer Science and Business Media.*

predominant mechanism of mass transport. An example of practical importance is Cr_2O_3.

3.9.2 Grain Boundary and Lattice Diffusion in Chromia Scales

Lattice diffusion has been measured in single crystal Cr_2O_3 and is found to be extremely slow. Several investigators [72—74] found that D_{Cr} was independent of p_{O_2} over a wide range, but increased with $p_{O_2}^{\frac{3}{4}}$ at high oxygen potentials, and perhaps [27] with $p_{O_2}^{-\frac{3}{4}}$ at low potentials. The oxygen potential effects are not well understood, although Kofstad [27] has suggested that Cr_2O_3 shows metal deficit behaviour at high p_{O_2} and metal excess behaviour at low p_{O_2}, and that the intermediate range where $D_{Cr} \neq f(p_{O_2})$ may reflect intrinsic behaviour. The most important finding, however, is the very low magnitude of D_{Cr}, 10^{-16} cm^2 s^{-1} at $p_{O_2} = 1$ atm and 1100°C. The activation energy for lattice diffusion of chromium is about 515 kJ mol^{-1}.

Chromium oxide scaling studies are restricted to relatively low temperatures to avoid volatilisation of both metal and oxide:

$$\mathrm{Cr(s)} = \mathrm{Cr(g)}, \quad \Delta G^{\circ} = 396,000 - 224\,\mathrm{T\ J\ mol^{-1}} \qquad [3.121]$$

$$\mathrm{Cr_2O_3} + \frac{1}{2}\mathrm{O_2} = 2\mathrm{CrO_3}, \quad \Delta G^{\circ} = 561,730 - 357\,\mathrm{T\ J\ mol^{-1}} \qquad [3.122]$$

Metal evaporation becomes important at temperatures above about 1000°C and CrO_3 formation at $p_{O_2} = 1$ atm is significant above 900°C. Even when consideration is restricted to low temperatures, the thermogravimetric kinetic data show a remarkable degree of scatter (Fig. 3.20).

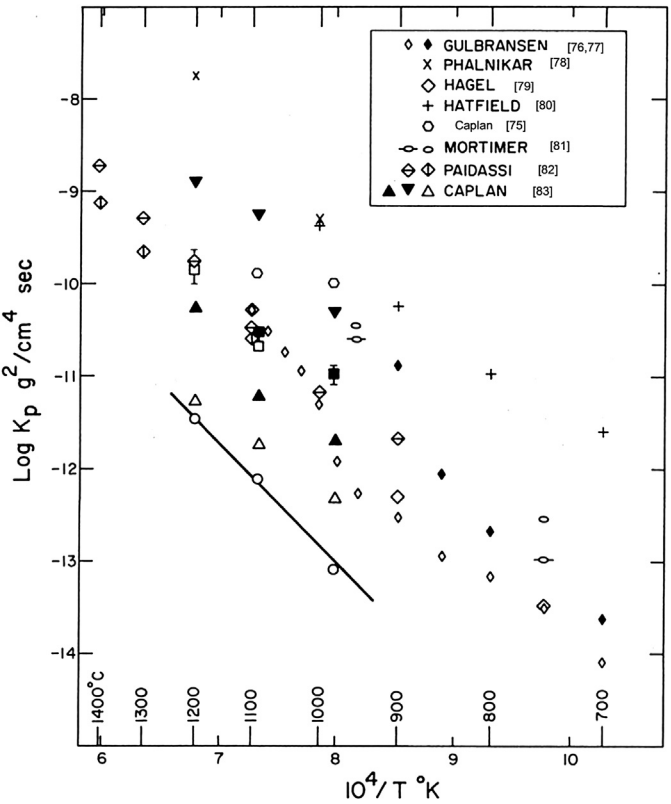

FIGURE 3.20 Comparison of reported rate constants for chromium oxidation. *With kind permission from D. Caplan, G.I. Sproule, Oxid. Met. 9 (1975) 459, Springer Science and Business Media.*

Caplan and Sproule [75] showed that much of the observed variation is due to the diversity of scale microstructures developed. These authors were able to use rather high temperatures by surrounding their samples with Cr_2O_3 to saturate the gas with CrO_3. As seen in Fig. 3.21, the scale grown on an etched polycrystalline chromium surface varied considerably, with thin oxide growing on some grains and thick oxide on others (and at grain boundaries). The figure compares SEM views of scale fracture sections taken from oxidised samples of etched and electropolished chromium. The latter is made up of multiple layers of detached, convoluted finely polycrystalline Cr_2O_3, whereas the former appears to be a single crystal of Cr_2O_3, still attached to the metal surface. The authors attributed these different outcomes to the very thin oxide left by the electropolishing procedure being finely polycrystalline, and nucleating a scale of similar microstructure [83]. The different morphological evolutionary paths of the two structures shown in Fig. 3.21 were accounted for in terms of their different diffusion mechanisms. The polycrystalline oxide grew rapidly, and developed compressive stresses, leading to convolution and eventual detachment from the metal. The compressive stresses were attributed to new oxide formation within the scale, resulting from simultaneous metal and oxygen diffusion along grain boundaries. The single crystal oxide scale grew slowly and developed no significant compressive stress because, in the absence of grain boundaries, only lattice diffusion of chromium occurred. In this case, a new oxide would form at the free outer surface, generating no stress.

The difference in observed weight change kinetics is clearly related to the different scale morphologies. However, the rate of supposedly single crystal scale growth was not quantitatively correlated with the lattice value of D_{Cr}, as there were no single crystal diffusion data available at that time. Because the

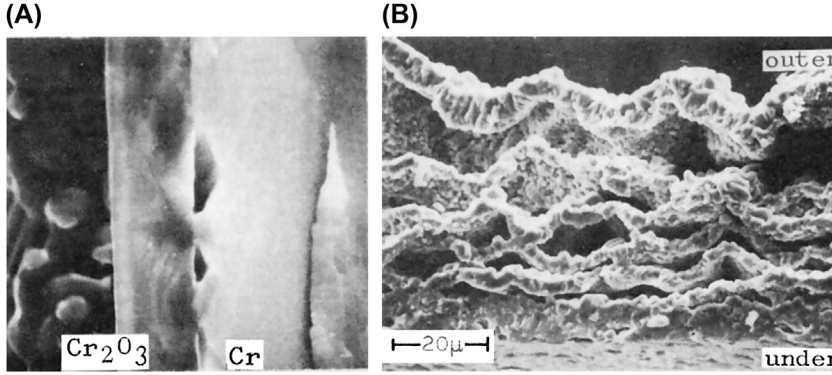

FIGURE 3.21 Fracture cross-sections of chromia scales grown at 1090°C on (A) etched Cr, and (B) electropolished Cr. *With kind permission from D. Caplan and G.I. Sproule, Oxid. Met. 9, 459 (1975), Springer Science and Business Media.*

diffusion coefficient is so small, data are still scant. If the value measured [74] at $p_{O_2} = 1$ atm and 1100°C of $D_{Cr} = 10^{-16}$ cm^2 s^{-1} is used in Eq. [3.84] with $p_{O_2} = 1$ atm, a value of $k_p = (m + 1) \times 10^{-16}$ cm^2 s^{-1} is predicted. The value measured by Caplan and Sproule at 1090°C corresponds to $k_p = 2 \times 10^{-13}$ cm^2 s^{-1}, three orders of magnitude faster. Moreover, the measured activation energy for oxidation was 240 kJ mol^{-1}, compared with 515 kJ mol^{-1} for diffusion. It would be concluded on this basis that lattice diffusion via cation vacancies cannot support the observed rate of chromia scale growth, even when no grain boundaries are present, and presumably lattice diffusion is important.

Consider now the possibility of scale growth supported by interstitial cation diffusion, in which case Eqs [3.90] and [3.94] should apply. We formulate the interstitial defect equilibrium

$$Cr_{Cr}^{\times} + \frac{3}{2}O_O^{\times} = Cr_i^{m\bullet} + me' + \frac{3}{4}O_2(g) \qquad [3.123]$$

along with the charge balance

$$C_e = mC_{Cr_i}$$

obtaining

$$C_{Cr_i} = \text{const.} p_{O_2}^{-3/4(m+1)} \qquad [3.124]$$

The value of p_{O_2} is that given by the Cr/Cr_2O_3 equilibrium. Using the value (Table 2.1) ΔH° (Cr_2O_3) = −746 kJ mol^{-1} of O_2, and Kofstad's [27] value of 515 kJ mol^{-1} for the diffusion activation energy, we find from Eq. [3.94] that the activation oxidation energy for oxidation is $[-550 + 746 \times 3/4\,(m + 1)]$ kJ mol^{-1}. If the interstitial species is singly charged, then the predicted activation energy is 236 kJ mol^{-1}, in close agreement with the 240 kJ mol^{-1} measured by Caplan and Sproule. Thus the temperature dependence is consistent with lattice diffusion via chromium interstitials. However, in the complete absence of diffusion data for the relevant regime of T and p_{O_2} and the lack of evidence for a singly charged interstitial chromium species, it would be unwise to view this agreement as conclusive.

The very low oxygen pressures needed to explore the behaviour of chromia near the Cr/Cr_2O_3 equilibrium can only be controlled by using H_2/H_2O or CO/CO_2 mixtures. Unfortunately, these molecular species have their own interactions with Cr_2O_3 [84−88], and these may obscure the oxygen effects which are relevant to chromia scales grown in pure oxygen. Data obtained [87] in H_2/H_2O atmospheres at 900°C corresponded to growth of Cr_2O_3 as the only reaction product under conditions where volatilisation would be slow. In this gas, $p_{O_2} = 1 \times 10^{-19}$ atm, and the rate constant was 8.6×10^{-11} g^2 cm^{-4} s^{-1}. Reference to Fig. 3.20 shows that this value is of the same order as other measurements made at $p_{O_2} = 1$ atm and much faster than the single crystal rate measured by Caplan and Sproule [75]. The fast rate is consistent with grain

boundary diffusion, and the lack of p_{O_2} dependence could indicate either that chromium interstitials are the mobile species or that some other species derived from H_2O was responsible for mass transfer.

Grain boundary transport in chromia scales is considered further in Section 7.3.3, for the case of alloy oxidation. Alumina scaling and the mechanisms of mass transport supporting it are discussed in Section 7.2.3.

3.9.3 Multilayer Scale Growth

As we have seen in Sections 2.2 and 3.2, multilayered scales can form during metal oxidation, and the scale structure is qualitatively predictable from the relevant phase diagram. Because local equilibrium is in effect at each of the interfaces, the values of a_o are fixed at these boundaries. Accordingly, we expect that the diffusion flux in each layer is inversely proportional to its thickness. However, we cannot evaluate layer thickening rates directly from these fluxes, because there is an additional mass transfer process at each interface. This problem has been treated by a number of authors [27,89–94].

Consider the growth of a duplex scale Fig. (3.22) made up of MO_a and MO_{a+b}. Under steady-state conditions, the thickness of each layer increases parabolically with time

$$X_i^2 = k_i t \qquad [3.125]$$

where k_i is a rate constant (which is not equal to k_p), and the subscript indicates the layer identity. The values of k_i depend on the diffusional fluxes in the oxide and on the interface reaction

$$MO_{a+b} + \frac{b}{a}M = \left(1 + \frac{b}{a}\right)MO_a \qquad [3.126]$$

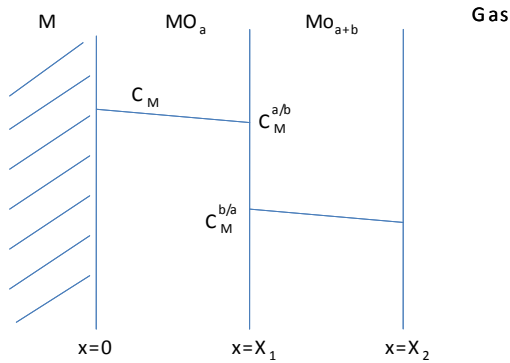

FIGURE 3.22 Schematic view of two-layered scale growth.

This situation can, in principle, be dealt with from a mass balance point of view. If metal is the only diffusing species,

$$J_1 - J_2 = \frac{dX_1}{dt}\left(C_{\mathrm{M}}^{b/a} - C_{\mathrm{M}}^{a/b}\right) \qquad [3.127]$$

where J_i is the metal flux in the indicated layer and $C_{\mathrm{M}}^{b/a}$, $C_{\mathrm{M}}^{a/b}$ are the concentrations of metal in the outer and inner oxide, respectively, both at the MO_a/MO_{a+b} interface. Evaluation of the J_i is difficult, and it is useful instead to relate the k_i values to other, simpler reactions.

If a single layer of MO_a is grown at $p_{O_2}(a,b)$, the equilibrium value for Eq. [3.126], the rate constant can be evaluated from Wagner's theory, assuming only metal diffuses, as

$$k_a = \int_{p'_{O_2}}^{p_{O_2}^{a/b}} \frac{Z_{\mathrm{M}}^{(1)}}{|Z_{\mathrm{o}}|} D_{\mathrm{M}}^{(1)} d \ln p_{O_2} \qquad [3.128]$$

The rate constant k_b is defined in terms of growth of a higher oxide layer on the surface of a lower oxide, in the absence of any base metal and therefore of diffusion from it, but exposed at its outer surface to $p_{O_2}(g) > p_{O_2}(a/b)$. This rate is related to the rate of outer layer thickening when both layers grow simultaneously on the metal, via the volume change accompanying the phase transformation [3.126]. Thus

$$k_b = (1 + a/b) f_2 \qquad [3.129]$$

$$f_b = \int_{p_{O_2}(a/b)}^{p_{O_2}(g)} \frac{Z_{\mathrm{M}}^{(2)}}{|Z_{\mathrm{o}}|} D_{\mathrm{M}}^{(2)} d \ln p_{O_2} \qquad [3.130]$$

Recognising that in the duplex scale relative layer thicknesses reflect the fractions of the metal flux consumed in growing each of them, it can be shown that

$$\frac{k_1}{k_2} = \frac{(X_1)^2}{(X_2)^2} \frac{1 + \alpha \frac{a}{a+b} \frac{X_2}{X_1}}{1 + \frac{1}{\alpha} \frac{X_1}{X_2}} \qquad [3.131]$$

where $\alpha = V_{MO_a}/V_{MO_{a+b}}$. Finally, the overall rate constant k^{ov} which describes the rate of total scale thickness increase is related to the layer growth rates by

$$k^{ov} = \left(k_1^{1/2} + k_2^{1/2}\right)^2 \qquad [3.132]$$

The applicability of this description to the growth of $FeO + Fe_3O_4$ scales on iron has been demonstrated by Garnaud and Rapp [95].

3.9.4 Development of Macroscopic Defects and Scale Detachment

As discussed in Section 2.10, oxide scale growth by outward metal transport leads to new oxide formation at the free outer surface, and no growth stresses result. However, as the metal surface recedes, the scale can maintain contact with it only if it is free to move. In the case of a flat sample of limited size, a rigid scale would be constrained at specimen edges and therefore unable to maintain contact. Even when the oxide has limited plasticity, growth of a sufficiently thick scale will eventually lead to detachment from the metal, starting at the edges. An example of the effect [96] is shown for a silver suphide scale in Fig. 3.23. The cross-section reveals that the sulphide had remained in contact with the flat sides of the specimen, forming a thick, compact scale as metal was consumed. Much less silver was reacted at the specimen edges, where geometrical constraints had prevented the sulfide from maintaining good contact. As seen in the figure, a porous reaction product had developed, rather than an empty gap.

This interpretation was confirmed by the 'pellet' experiment [97,98] shown schematically in Fig. 3.24. A pellet of the same material as the scale was placed in contact with the metal specimen. A tube containing the oxidant (liquid sulphur in this case) was placed on top of the pellet and held there under load. Heating the whole assembly was found to cause growth of more scale up into the tube (confirming outward diffusion of silver in Ag_2S). As the metal was consumed, the pellet and loaded tube moved downward, maintaining contact with the metal. No region of porous sulfide developed. However, if at some time after commencement of the reaction, the metal and tube of sulphur were each independently clamped in position, porous sulfide formed at the pellet-metal interface.

The development of porous material was described by Mrowec and coworkers [96] using their dissociation mechanism. Once local scale-metal separation occurs, the metal activity at the underside of the scale can no longer be maintained. Metal continues to diffuse outward, driven by the oxidant chemical potential gradient, and a_M decreases. Consequently, as seen from Eq. [3.82], a_o increases, and gas-phase transport commences from the

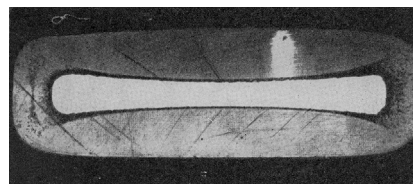

FIGURE 3.23 Cross-section of flat silver sample after sulphidation at 444°C for 9 min [96].

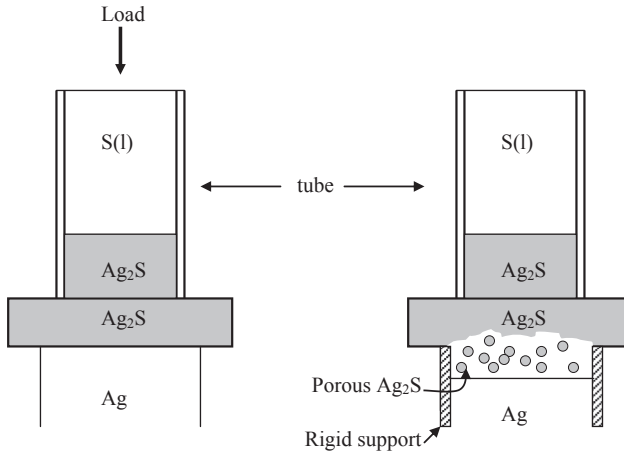

FIGURE 3.24 Schematic illustration of Rickert's [97,98] pellet experiment. Description in text.

underside of the scale to the underlying metal surface. A porous product grows under gaseous mass transfer control, until it bridges the gap between metal and separated scale, whereupon outward metal transport resumes.

As calculated in Section 2.9 (and as pointed out by Gibbs [99]), the oxidant partial pressures prevailing at metal-scale interfaces are usually too low to support any significant transport. However, as diffusion through the scale takes place, the a_o value at the scale underside will rise and gaseous mass transport could thereby be enabled. Birks and Rickert [61] showed that in the case of NiO growth, the likely p_{O_2} values were sufficient to account for the observations. Furthermore, most metals contain carbon impurities which will oxidise. As shown by Graham and Caplan [100], the resulting CO/CO_2 mixture occupies the voids. In this case, the gas can act as an oxygen carrier via the reactions

$$CO + MO = CO_2 + M$$

taking place in different directions on opposite sides of the cavity (Fig. 3.25).

Finally, it will be recalled that real oxide scales are polycrystalline, and inward oxygen diffusion via grain boundaries can occur. Atkinson et al. [69] used ^{18}O tracer studies to show that oxygen did not penetrate NiO scales during their initial growth, but that long-term penetration occurred when an inner, porous NiO scale sublayer developed. This transport of oxidant molecules is suggested to take place through microchannels or pores developed in the outer layer. Mrowec and co-workers [96] have proposed that the underside of a separated scale will dissociate preferentially at oxide grain boundaries, where outward diffusion of metal is fastest. This process could then create

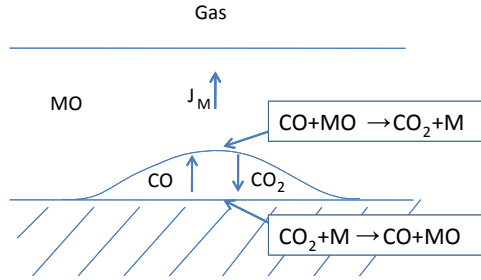

FIGURE 3.25 Action of CO/CO_2 couple within a void accelerating oxygen transport.

microchannels along favourably oriented boundaries, allowing subsequent inward transport of molecular oxidant. The possibility of molecular species penetrating scales is discussed in Chapters 4, 9, 10 and 11.

3.10 REACTIONS NOT CONTROLLED BY SOLID-STATE DIFFUSION

As observed in Section 1.6, parabolic scaling kinetics are not invariably observed at high temperatures, and processes other than solid-state diffusion can control the reaction rate. For pure metals, this will be the case if either an interfacial process or gas-phase mass transfer is slower than diffusion in the scale. The principles involved are discussed here with reference to the oxidation of iron and silicon at low oxygen potentials.

3.10.1 Oxidation of Iron at Low p_{O_2} to Form Wüstite Only

Linear scaling kinetics have long been reported [101] for the oxidation of iron at low oxygen potentials where only $Fe_{1-\delta}O$ forms. In order to obtain the low p_{O_2} values required, gas mixtures of $CO-CO_2$ or H_2-H_2O are used. Because the p_{O_2} values are so low (10^{-15} to 10^{-13} atm at 1000°C), molecular oxygen is far less abundant than the CO_2 or H_2O species. Given that the homogeneous gas-phase dissociation reactions of both CO_2 and H_2O are rather slow at these temperatures, it is clear that the relevant species of importance are CO_2 and H_2O. In the case of CO_2, the linear rate was found to depend on p_{O_2} and the total pressure of $CO + CO_2$ mixtures [52,102–108]. It was concluded that the rate was controlled by the reaction

$$CO_2(g) + S = CO(g) + O|S \qquad [3.133]$$

where, as before, S represents a surface adsorption site, and the net rate can be written

$$\text{Rate} = k_f p_{CO_2} \theta_v - k_r p_{CO}(1 - \theta_v) \qquad [3.134]$$

with k_f, k_r denoting the forward and reverse rate constants for Eq. [3.133], and θ_v the fraction of surface sites empty. At the Fe/FeO equilibrium oxygen

activity, a_o^*, the net rate is zero. Substituting from the CO/CO_2 equilibrium expression Eq. [2.15]

$$a_o^* = K_c \frac{p_{CO_2}}{p_{CO}} \quad [3.135]$$

into Eq. [3.134], we obtain from the zero rate condition the general result

$$k_r(1-\theta_v) = k_f \theta_v \frac{a_o^*}{K_c} \quad [3.136]$$

enabling us to rewrite Eq. [3.134] as

$$\text{Rate} = k_f \theta_v \left[p_{CO_2} - \frac{a_o^*}{K_c} p_{CO} \right] \quad [3.137]$$

In gas mixtures containing only CO and CO_2

$$P_T = p_{CO} + p_{CO_2} \quad [3.138]$$

and

$$\text{Rate} = k_1 \theta_v P_T \left[N_{CO_2} \left(1 + a_o^*/K_c\right) - a_o^*/K_c \right] \quad [3.139]$$

where $N_{CO_2} = p_{CO_2}/P_T$. As seen in Fig. 3.26, the data of Pettit et al. [102] confirm the dependence on both total pressure and CO_2 mol fraction, providing that θ_v is constant. A similar expression has been shown to apply for the linear kinetics of wüstite scaling in H_2/H_2O atmospheres [52]. Grabke

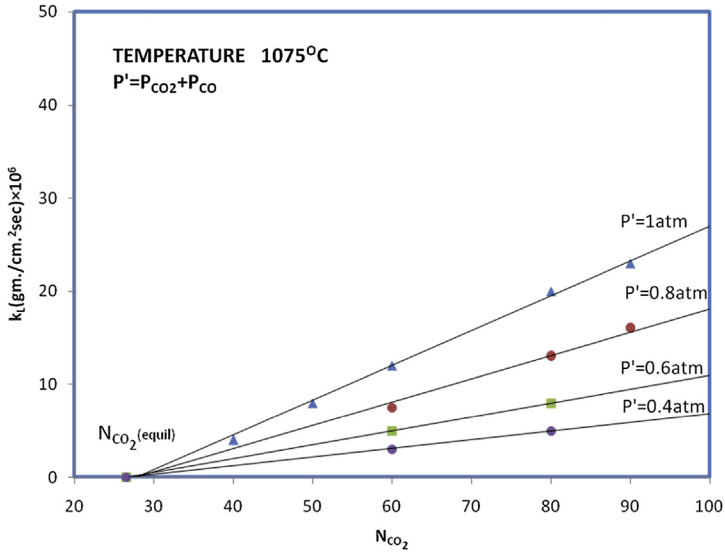

FIGURE 3.26 Dependence of initial linear iron oxidation rate on composition and total pressure in CO/CO_2 mixtures. *Reprinted from F. Pettit, R. Yinger, J.B. Wagner, Jr., Acta Metall. 8 (1960) 617, with permission from Elsevier.*

[109] showed that the linear rate constant values in CO/CO_2 atmospheres agreed with those obtained for surface exchange of oxygen on wüstite equilibrated with iron.

As the wüstite scale thickens, diffusion through it slows until a thickness is reached at which diffusion becomes rate-controlling and the kinetics parabolic [52]. It has been noted [104,106] that reaction at high p_{CO_2} values produces scales of wüstite only, although the equilibrium p_{O_2} values calculated from Eq. [2.15] exceed the value for Fe_3O_4 formation. Clearly the supposed gas-phase equilibrium is not in effect, and instead the local CO/CO_2 ratio is set at the gas-scale boundary. As noted by Kofstad [27], parabolic scaling in H_2/H_2O gases is faster than in CO/CO_2 gases of the same calculated equilibrium oxygen potential. Again this indicates that the scale-gas boundary conditions cannot be calculated from the $CO-CO_2$ equilibrium. Part of the reason for this is the rapid rate at which oxygen is incorporated into the fast growing scale.

As shown in Section 2.9, the oxidation of low carbon steels in substoichiometric combustion gases leads to wüstite scale formation according to linear kinetics. Mass transfer calculations showed that gas-phase mass transfer did not control the rate, but a surface reaction process did. A regime of behaviour was found for low carbon, low silicon steel [110] in which a small fractional change in oxidant partial pressure led to a relatively large change in rate, as shown in Fig. 3.27. The expression, in Eq. [3.139], cannot be used because $\left(p_{CO_2} + p_{CO}\right) \neq$ constant. Even Eq. [3.137] is unreliable, because θ_v can vary, and a different treatment of the surface processes is to be preferred.

The surface reactions are reformulated as

$$\begin{aligned} &CO_2(g) + S = CO_2|S && \text{(a)} \\ &CO_2|S \underset{k_{-1}}{\overset{k_1}{\rightleftarrows}} O|S + CO(g) && \text{(b)} \\ &O|S \xrightarrow{k_2} O_o^X + S && \text{(c)} \end{aligned}$$

in order to track vacant surface sites. Assuming a fixed concentration of surface sites

$$M = [S] + [O|S] + [CO_2|S] \qquad [3.140]$$

defining K_a as the adsorption equilibrium constant for reaction (a) and using the rate constants specified in reactions (b) and (c), we formulate the steady-state approximation for the surface concentration $[O|S]$:

$$\frac{d[O|S]}{dt} = 0 = k_1[CO_2|S] - k_{-1}[O|S]p_{CO} - k_2[O|S] \qquad [3.141]$$

It is found by substituting $K_a p_{CO_2}[S]$ for $[CO_2|S]$ in Eqs [3.140] and [3.141], followed by elimination of [S], that

$$[O|S] = \frac{k_1 K_a M p_{CO_2}}{K_a p_{CO_2}(k_1 + k_{-1}p_{CO} + k_2) + k_{-1}p_{CO} + k_2} \qquad [3.142]$$

A similar scheme can be proposed for reaction with H_2O.

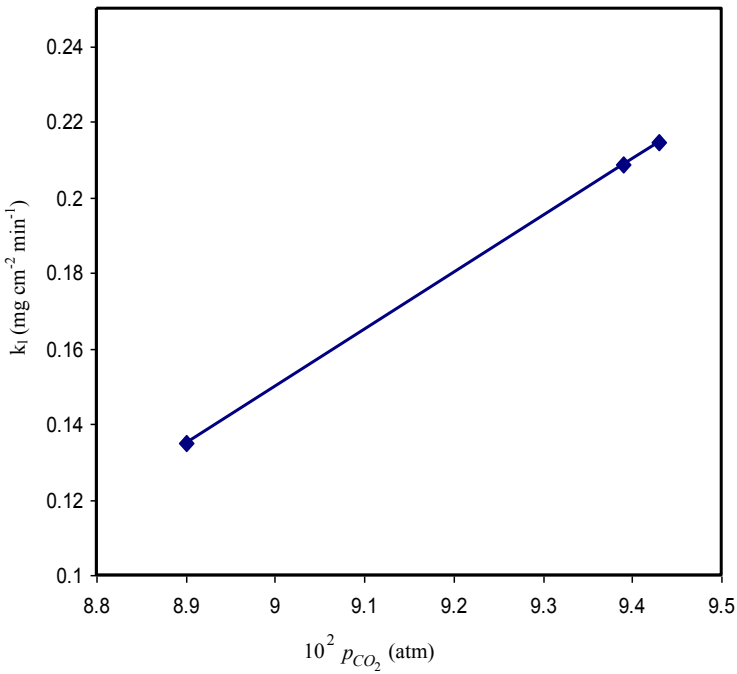

FIGURE 3.27 Linear scaling rates for a low carbon steel in simulated reheat furnace gas, $T = 1100°C$. *With kind permission from V.H.J. Lee, B. Gleeson, D.J. Young, Oxid. Met. 63 (2005), 15, Springer Science and Business Media.*

The rate of the oxygen uptake reaction (c) is proportional to [O|S], given by Eq. [3.142]. It is concluded then that k_2 is not the dominant term in the numerator (because the reaction rate is not proportional to p_{CO_2}) and the reverse of reaction (b) must therefore be significant. Similarly, it can be concluded that the surface is not saturated with adsorbed CO_2, as the rate does change with changing gas compositions, and therefore $K_a p_{CO_2}$ cannot be large. Proceeding on the assumption that, in fact, $K_a p_{CO_2}$ is small, Eq. [3.142] is approximated as

$$[\mathrm{O|S}] = \frac{k_2 K_a \mathrm{M} p_{CO_2}}{k_2 - k_{-1} p_{CO}} \qquad [3.143]$$

and the oxidation rate expression becomes

$$k_l = \frac{p_{CO_2}}{a + b p_{CO}} \qquad [3.144]$$

where a and b are constants. This expression was found to fit the data well [110] with $a = 0.375\ \mathrm{mg}^{-1}\ \mathrm{cm}^2\mathrm{s\ atm}$ and $b = 27.3\ \mathrm{mg}^{-1}\ \mathrm{cm}^2\mathrm{s}$. The large change in p_{CO} had a much greater effect than did the very small one in p_{CO_2}.

Yet another regime of behaviour is found for iron oxidation in the case of exposure to dilute oxygen-bearing gases. Abuluwefa et al. [111] oxidised a low carbon, low silicon steel in N_2-O_2 mixtures containing 1−16% O_2, at temperatures of 1000−1250°C. They found initially linear rates, followed by steady-state parabolic kinetics. The linear rate constant was directly proportional to p_{O_2} and displayed a very small activation energy, 17 kJ mol^{-1}. The observed scaling rates were in good agreement at low p_{O_2} values with predictions made for gas-phase diffusion control using Eq. [2.157], as shown in Fig. 3.28. The small activation energy is also consistent with such a mechanism. The difference between this situation and the combustion gas oxidation discussed above was the larger total oxidant partial pressures of the latter, leading to higher gaseous transfer rates.

3.10.2 Oxidation of Silicon

As seen earlier, scales of amorphous SiO_2 are extremely slow growing and provide excellent protection. However, volatile species can form at elevated temperatures, causing wastage of silicon.

Partial pressures of the various possible gas species are shown in Fig. 3.29, where p_{SiO} is seen to reach a maximum near the Si/SiO_2 equilibrium oxygen partial pressure. At lower values of p_{O_2}, SiO(g) forms and, in the absence of a protective silica scale, silicon is lost through this volatilisation process. Wagner [57] analysed this phenomenon, which he called 'active' oxidation, in terms of gas-phase mass transfer. Because oxygen is consumed at the silicon

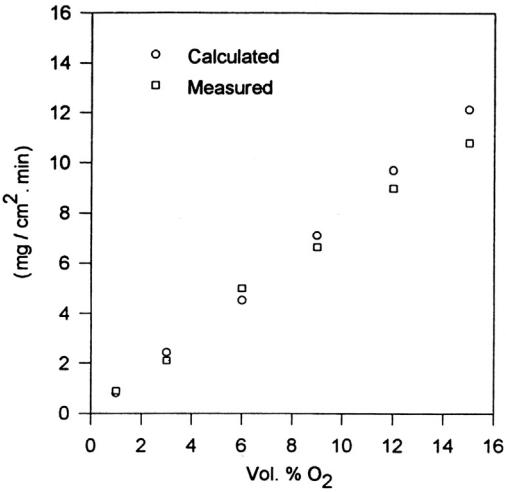

FIGURE 3.28 Comparison of measured rates for carbon steel oxidation at 1200°C with values calculated from Eq. [2.157]. *With kind permission from H. Abuluwefa, R.I.L. Guthrie, F. Ajersch, Oxid. Met. 46 (1996), 423, Springer Science and Business Media.*

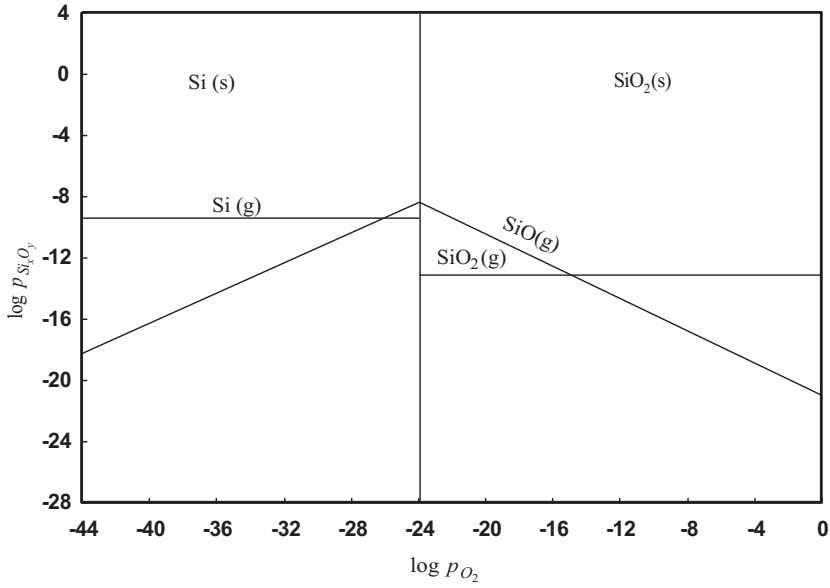

FIGURE 3.29 Equilibrium vapour pressures in the Si-O system at $T = 1127°C$.

surface, a diffusion gradient is established in the gas mixture near the surface (Fig. 3.30). Thus the value at the surface, $p^*_{O_2}$, could be below the minimum necessary for solid SiO_2 formation, even with a p_{O_2} (gas) value above it. It is recognised that the initial value of p_{O_2} (gas) necessary to passivate the silicon

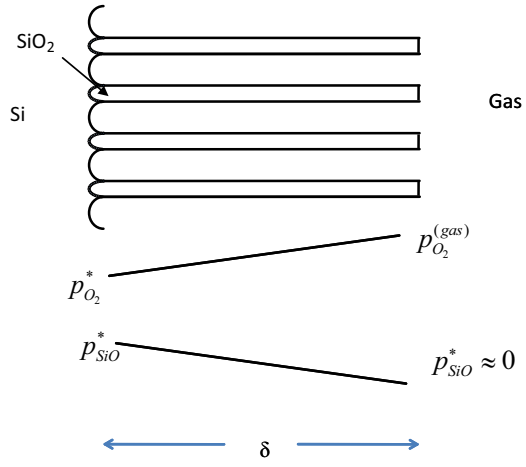

FIGURE 3.30 Filamentary SiO_2 growth on silicon at high temperatures, showing gas-phase partial pressure gradients.

surface is therefore higher than the equilibrium Si/SiO_2 value. The critical value can be calculated from a consideration of gas-phase mass transfer.

Most situations of practical interest involve the viscous flow regime, and Eqs [2.157] and [2.158] apply. To use them, we need boundary values for both p_{O_2} and p_{SiO}, which are related via local equilibrium at the silicon-gas interface

$$Si(s) + \frac{1}{2}O_2(g) = SiO(g) \qquad [3.145]$$

$$p^*_{SiO} = K\left(p^*_{O_2}\right)^{\frac{1}{2}} \qquad [3.146]$$

From Eq. [2.157]

$$J_{O_2} \approx \frac{k_{O_2} p_{O_2}}{RT} = \frac{D_{O_2} p_{O_2}}{\delta_{O_2} RT} \qquad [3.147a]$$

$$J_{SiO} = \frac{D_{SiO} p_{SiO}}{\delta_{SiO} RT} \qquad [3.147b]$$

where δ is the thickness of the boundary layer (Fig. 3.30). The steady-state condition for SiO volatilisation is

$$J_{SiO} = 2J_{O_2} \qquad [3.148]$$

and therefore

$$p_{O_2} = \frac{1}{2}\frac{\delta_{O_2}}{\delta_{SiO}}\frac{D_{SiO}}{D_{O_2}} p_{SiO} \qquad [3.149]$$

It can be shown that for a laminar boundary layer

$$\delta_{SiO}/\delta_{O_2} \approx (D_{SiO}/D_{O_2})^{\frac{1}{2}} \qquad [3.150]$$

and Eq. [3.149] becomes

$$p_{O_2} = \frac{1}{2}\left(\frac{D_{SiO}}{D_{O_2}}\right)^{\frac{1}{2}} p_{SiO} \qquad [3.151]$$

Consider now the critical condition for protective SiO_2 formation

$$\frac{1}{2}Si(s) + \frac{1}{2}SiO_2(s) = SiO(g) \qquad [3.152]$$

which defines an equilibrium value, p^{Eq}_{SiO}. The critical value of p_{O_2} is therefore given by

$$p_{O_2}(crit) = \frac{1}{2}\left(\frac{D_{SiO}}{D_{O_2}}\right)^{\frac{1}{2}} p^{Eq}_{SiO} \qquad [3.153]$$

If the gas phase p_{O_2} is higher, then protective SiO_2 forms. If it is lower, p^*_{SiO} adjusts through Eq. [3.146], and volatilisation or active oxidation results.

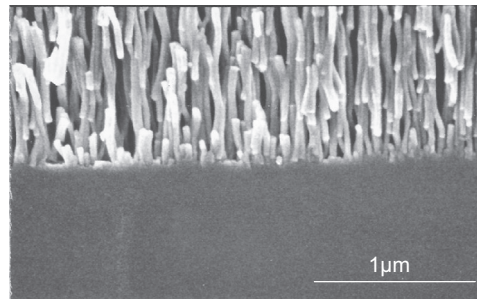

FIGURE 3.31 Silica nanofibres formed by oxidation of silicon at 1130°C in CO/CO_2. *With kind permission from P. Carter, B. Gleeson, D.J. Young, Oxid. Met. 56 (2001) 375, Springer Science and Business Media.*

A similar analysis can be made for the molecular flow regime, using Eq. [2.155]. Its effectiveness in predicting the transition between active and protective oxidation has been verified experimentally [112–114]. Behaviour in the viscous flow regime is more complex, however, because when solid SiO_2 does form, it can be in the form of a nonprotective, fast growing deposit. Hinze and Graham [115] observed three regimes of behaviour in $Ar–O_2$ mixtures at 1227°C: linear weight loss at low p_{O_2}, fast linear weight gain at somewhat higher p_{O_2} and protective oxidation at $p_{O_2} \geq 4 \times 10^{-3}$ atm. The explanation for the intermediate regime was suggested to be formation of SiO_2 whiskers growing from the silicon surface. The outer tips of these whiskers acted as growth sites, redefining the diffusion distance δ_{SiO} (Fig. 3.30) and explaining the rapid reaction through an accelerated SiO flux Eq. [3.147b].

Improved imaging capabilities, which have become available since that work, have allowed the production of Fig. 3.31. A highly ordered structure of SiO_2 is seen to develop [116] in confirmation of the Hinze and Graham proposal.

3.11 THE VALUE OF THERMODYNAMIC AND KINETIC ANALYSIS

In this chapter, we have explored the application of thermodynamic and kinetic analysis techniques to the simplest high temperature oxidation situation: reaction of a pure metal with a single oxidant. It is clear that the usual hypothesis of local equilibrium at interfaces between contacting phases is commonly correct. Thus the oxide (or sulfide, etc.) predicted to be at equilibrium with the gas is usually found at the scale surface; the oxide shown by the phase diagram to equilibrate with the metal is found to grow in contact with the metal. When this is not so, it can be concluded that solid-state diffusion does not control the reaction rate, and that instead either a

gas-phase process or a surface reaction is rate controlling. Calculation of gas-phase mass transfer rates has been found to be quantitatively successful in determining when these processes are capable of controlling the rate.

More importantly, the model of local equilibrium within the growing oxide scale is also successful. The state of a scale interior is well-described as a series of microscopic local equilibrium regions, each incrementally different (in the growth direction) from adjacent regions, as shown schematically in Fig. 3.32. This allows the use of the diffusion path description and justifies the application of irreversible thermodynamics to the diffusion problem.

In a very large number of cases, scale growth is controlled by solid-state diffusion. The Wagner treatment of this situation is found to succeed when adequate information on oxide defect properties is available. This success provides proof that lattice diffusion of point defect species can support scale growth in a number of cases. It leads to very useful predictions as to how the scaling rate will vary with oxide type (degree of nonstoichiometry and lattice species mobility) and with oxidant activity and temperature. It also succeeds in predicting qualitatively the effect of dilute oxide solute impurities on scaling rates.

The value of the Wagner treatment is less obvious in the case of slow-growing oxides such as Cr_2O_3 and Al_2O_3. Our knowledge of the defect properties of these oxides, and the effect of oxygen potential upon them, is very limited, and testing the Wagner model is in this sense difficult. Moreover, as is discussed in Chapter 7, the diffusion properties of these oxides are often dominated by grain boundary transport. As seen in Section 3.9, grain boundary

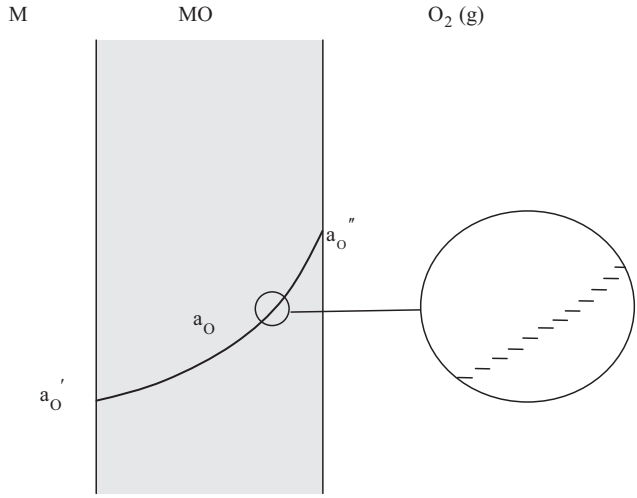

FIGURE 3.32 The local equilibrium description: a series of very small regions each of which can be approximated as homogeneous.

diffusion can lead to oxidation rates very different from those predicted by Wagner and even to different kinetics when microstructural change occurs with time. The Hart Eq. [3.113], which is so widely used to describe grain boundary diffusion, is in fact only accurate for the case of prismatic grains aligned parallel to the diffusion direction. The Maxwell Equation

$$D_{\text{eff}} = \frac{D_{\text{B}}((3-2f)D_{\text{L}} + 2fD_{\text{B}})}{fD_{\text{L}} + (3-f)D_{\text{B}}} \qquad [3.154]$$

was derived some time ago [117,118] as part of a more general field theory. More recently, it has been shown [119] to yield more accurate predictions than the Hart equation for a diversity of grain shapes and orientations.

Notwithstanding the grain boundary contribution, the mass transfer mechanism is still one of diffusion, and the basic concepts underlying Wagner's theory still provide insight and a basis for experimental design. To obtain value from the theory, however, it is essential to add to it a detailed description of microstructural phenomena. Arriving at a definitive version of such a description is a continuing preoccupation in high temperature corrosion research. For this reason, microstructural evolution receives considerable attention in the remainder of this book.

REFERENCES

[1] J. Paidassi, Rev. Met. 54 (1957) 569.
[2] D.W. Bridges, J.P. Baur, W.M. Fassel, J. Electrochem. Soc. 103 (1956) 619.
[3] D. Caplan, M.J. Graham, M. Cohen, J. Electrochem. Soc. 119 (1972) 1205.
[4] D. Caplan, G.I. Sproule, Oxidation Met. 9 (1975) 459.
[5] T. Narita, K. Nishida, Trans. Jpn. Inst. Met. 14 (1973), 439, 447.
[6] D. Coutsouradis, A. Davin, in: Z.A. Foroulis (Ed.), High Temperature Corrosion by Sulfur and its Compounds, Electrochemical Society Inc., New York, 1970, p. 132.
[7] B.D. Bastow, G.C. Wood, Oxid. Met. 9 (1975) 473.
[8] D.J. Young, W.W. Smeltzer, J. Electrochem. Soc. 123 (1976) 232.
[9] C. Wagner, Z. Phys. Chem. 21 (1933) 25.
[10] F.A. Kroger, H.J. Vink, Solid State Phys. 3 (1956) 307.
[11] F.A. Kroger, F.H. Stieltjes, H.J. Vink, Philips Res. Repts. 14 (1959) 557.
[12] I. Frenkel, Z. Physik. 35 (1926) 652.
[13] W. Schottky, C. Wagner, Z. Phys. Chem. B11 (1950) 163.
[14] W. Jost, J. Chem. Phys. 1 (1933) 466.
[15] N.N. Greenwood, Ionic Crystals, Lattice Defects and Nonstoichiometry, Chemical Publishing Company, New York, 1970.
[16] C. Wagner, Atom Movements, ASM, Cleveland, 1951, p. 153.
[17] D.J. Young, F. Gesmundo, High Temp. High Press 20, 1988, p. 1.
[18] C. Wagner, Prog. Solid State Chem. 10 (1975) 3.
[19] D.J. Young, Scripta Met. 9 (1975) 159.
[20] J.S. Kirkaldy, D.J. Young, Diffusion in the Condensed State, Institute of Metals, London, 1987.
[21] M.L. Volpe, J. Reddy, J. Chem. Phys. 53 (1970) 1117.

[22] M.L. Volpe, N.L. Peterson, N. Lee, J. Reddy, Phys. Rev. B 3 (1971) 1417.
[23] W.C. Tripp, N.M. Tallan, J. Am. Ceram. Soc. 53 (1970) 531.
[24] B. Fisher, D.S. Tannhauser, J. Chem. Phys. 44 (1966) 1663.
[25] R.E. Carter, F.D. Richardson, Trans. AIME 200 (1954) 1244.
[26] R.E. Carter, F.D. Richardson, Trans. AIME 203 (1955) 336.
[27] P. Kofstad, High Temperature Corrosion, Elsevier Applied Science, London, 1988.
[28] K. Fueki, J.B. Wagner, J. Electrochem. Soc. 112 (1965) 384.
[29] S. Mrowec, T. Walec, T. Werber, Corros. Sci. 6 (1966) 287.
[30] S. Mrowec, K. Przybylski, Oxid. Met. 11 (1977) 365.
[31] W.R. Chen, N.L. Peterson, W.T. Reeves, Phys. Rev. 186 (1969) 887.
[32] F. Gesmundo, F. Viani, J. Electrochem. Soc. 128 (1981) 460.
[33] W.W. Smeltzer, D.J. Young, Prog. Solid State Chem. 10 (1975) 17.
[34] J.H. Swisher, E.T. Turkdogan, Trans. AIME 239 (1967) 426.
[35] L. Himmel, R.F. Mehl, C.E. Birchenall, Trans. AIME 197 (1953) 827.
[36] A.G. Goursat, W.W. Smeltzer, J. Electrochem. Soc. 120 (1973) 390.
[37] S.M. Klotsman, A.N. Timobeyev, I. Sh, Traktenberg. Phys. Met. Metall. 10 (1960) 93.
[38] R. Lundner, Arkiv Kemi 4 (1952) 381.
[39] W.C. Hagel, Trans. AIME 236 (1966) 179.
[40] W.W. Smeltzer, Acta Met. 8 (1960) 377.
[41] H.J. Engell, Acta Met. 6 (1958) 439.
[42] M.H. Davies, M.T. Simnad, C.E. Birchenall, Trans. AIME 191 (1951) 889.
[43] N.G. Schmall, H. Baumann, H. Schenck, Arch. Eisenhutten 29 (1958) 83.
[44] P. Kofstad, A.Z. Hed, J. Electrochem. Soc. 115 (1968) 102.
[45] P. Vallet, P. Raccah, Mem. Sci. Rev. Met. 62 (1965) 1.
[46] F. Koch, J.B. Cohen, Acta Crystallog. B25 (1969) 275.
[47] D.J. Young, Rev. High Temp. Mater. 4 (1980) 299.
[48] R.H. Condit, R.R. Hobbins, C.E. Birchenall, Oxid. Met. 8 (1974) 409.
[49] P. Toulmin, P.B. Barton, Geochim. Cosmochim. Acta 28 (1964) 641.
[50] E.M. Fryt, V.S. Bhide, W.W. Smeltzer, J.S. Kirkaldy, J. Electrochem. Soc. 126 (1979) 683.
[51] E.M. Fryt, W.W. Smeltzer, J.S. Kirkaldy, J. Electrochem. Soc. 126 (1979) 673.
[52] F.S. Pettit, J.B. Wagner, Acta Met. 12 (1964) 35.
[53] E.T. Turkdogan, W.M. McKewan, L. Zwell, J. Phys. Chem. 69 (1965) 327.
[54] C. Wagner, K. Grunewald, Z. Phys. Chem. 40B (1938) 455.
[55] B.E. Deal, A.S. Grove, J. Appl. Phys. 36 (1965) 3770.
[56] A.G. Revesz, B.J. Mrstik, H.L. Hughes, D. McCarthy, J. Electrochem. Soc. 133 (1986) 31.
[57] R.A. Rapp, Met. Trans. A A15 (1984) 765.
[58] K. Nagel, C. Wagner, Z. Phys. Chem. B40 (1939) 455.
[59] C. Wagner, Z. Phys. Chem. B32 (1936) 447.
[60] C.S. Giggins, F.S. Pettit, Trans. AIME 245 (1969) 2495.
[61] N. Birks, H. Rickert, J. Inst. Met. 91 (1962) 308.
[62] F.A. Kröger, The Chemistry of Imperfect Crystals, North-Holland, Amsterdam, 1964.
[63] R. Herchl, N.N. Khoi, T. Homma, W.W. Smeltzer, Oxid. Met. 4 (1972) 35.
[64] J.M. Perrow, W.W. Smeltzer, J.D. Embury, Acta Met. 16 (1968) 1209.
[65] I. Kaur, W. Gust, Fundamentals of Grain and Interphase Boundary Diffusion, Ziegler Press, Stuttgart, 1989.
[66] E.W. Hart, Acta Met. Metall. 5 (1957) 597.
[67] W.W. Smeltzer, R.R. Haering, J.S. Kirkaldy, Acta Metall. 9 (1961) 880.
[68] M.J. Graham, D. Caplan, M. Cohen, J. Electrochem. Soc. 119 (1972) 1265.

[69] A. Atkinson, R.I. Taylor, P.D. Goode, Oxid. Met. 13 (1979) 519.
[70] A. Atkinson, R.I. Taylor, A.E. Hughes, in: R.A. Rapp (Ed.), High Temperature Corrosion, NACE, Houston, TX, 1983, p. 110.
[71] A. Atkinson, M.L. Dwyer, R.I. Taylor, J. Mater. Sci. 18 (1983) 2371.
[72] K. Hoshino, N.L. Peterson, J. Am. Ceram. Soc. 66 (1983) C202.
[73] D.R. Kinloch, (Ph.D. thesis), Quoted in Ref. 26, p 116.
[74] A. Atkinson, R.I. Taylor, in: Proc. 3rd Int. Conf, Nonstoichiometric Compounds, State College, PA, 1984.
[75] D. Caplan, G.I. Sproule, Oxid. Met. 9 (1975) 459.
[76] E.A. Gulbransen, K.F. Andrew, J. Electrochem. Soc. 99 (1952) 402.
[77] E.A. Gulbransen, K.F. Andrew, J. Electrochem. Soc. 104 (1957) 334.
[78] C.A. Phalnikar, E.B. Evans, W.M. Baldwin, J. Electrochem. Soc. 103 (1956) 429.
[79] W.C. Hagel, Trans. ASM 56 (1963) 583.
[80] W.H. Hatfield, JISI London 115 (1927) 483.
[81] D. Mortimer, M.L. Post, Corros. Sci. 8 (1968) 499.
[82] L. Cadiou, J. Paidassi, Mem. Sci. Rev. Metall. 66 (1969) 217.
[83] D. Caplan, A. Harvey, M. Cohen, Corros. Sci. 9 (1963) 161.
[84] K.P. Lillerud, P. Kofstad, Oxid. Met. 17 (127) (1982) 177−195.
[85] T. Norby, Advan. Ceram. 23 (1987) 107.
[86] T. Norby, J. Phys. IV (3) (1993) 99.
[87] X.G. Zheng, D.J. Young, Oxid. Met. 42 (1994) 163.
[88] W.J. Quadakkers, J.F. Norton, S. Canetoni, K. Schuster, A. Gil, in: Proc. 3rd Conf. Microscopy of Oxidation, 1996, p. 609.
[89] G. Valensi, Rev. Metall. 45 (1948) 205.
[90] C. Wagner, Acta Met. 17 (1969) 99.
[91] G.J. Yurek, J.P. Hirth, R.A. Rapp, Oxid. Met. 8 (1976) 265.
[92] F. Gesmundo, F. Viani, Corros. Sci. 18 (217) (1978) 231.
[93] H.S. Hsu, Oxid. Met. 26 (1986) 315.
[94] G. Wang, B. Gleeson, D.L. Douglass, Oxid. Met. 31 (1989) 415.
[95] G. Garnaud, R.A. Rapp, Oxid. Met. 11 (1977) 193.
[96] S. Mrowec, T. Werber, Gas Corrosion of Metals, US National Bureau of Standards, Nat. Center Sci. Tech. Economic Information, Warsaw, 1978.
[97] H. Rickert, Z. Phys. Chem. N.F. 21 (1959) 432.
[98] H. Rickert, C. Wagner, Z. Phys. Chem. N.F. 31 (1961) 32.
[99] G.B. Gibbs, Oxid. Met. 7 (1973) 173.
[100] M.J. Graham, D. Caplan, J. Electrochem. Soc. 120 (1972) 843.
[101] K. Fischbeck, L. Neundeubel, F. Salzer, Z. Elektrochem. 40 (1934) 517.
[102] F. Pettit, R. Yinger, J.B. Wagner Jr., Acta Metall. 8 (1960) 617.
[103] K. Hedden, G. Lehmann, Arch. Eisenhüttenwes 35 (1964) 839.
[104] W.W. Smeltzer, Acta Metall. 8 (1960) 377.
[105] H.J. Grabke, Ber. Bunsenges. Phys. Chem. 69 (1965) 48.
[106] P. Kofstad, R. Bredsen, in: Proc. 9th Int. Congr. on Metallic Corrosion, vol. 1, Nat. Res. Council of Canada, Ottawa, June 1984, p. 12.
[107] W.W. Smeltzer, A.G. Goursat, Rev. High Temp. Mater. 1 (1973) 351.
[108] K. Hauffe, H. Pfeiffer, Z. Metallkunde 44 (1953) 27.
[109] H.J. Grabke, in: Proc. 3rd Int. Congr. 2, Catalysis, Amsterdam, 1964, p. 928.
[110] V.H.J. Lee, B. Gleeson, D.J. Young, Oxid. Met. 63 (2005) 15.
[111] H. Abuluwefa, R.I.L. Guthrie, F. Ajersch, Oxid. Met. 46 (1996) 423.

[112] E.A. Gulfransen, S.A. Jansson, Oxid. Met. 4 (1972) 181.
[113] J.E. Antill, J.B. Warburton, Corros. Sci. 11 (1971) 337.
[114] C. Gelain, A. Cassuto, P. De Goff, Oxid. Met. 3 (1971) 139.
[115] J.W. Hinze, H.C. Graham, J. Electrochem. Soc. 123 (1986) 1066.
[116] P. Carter, B. Gleeson, D.J. Young, Oxid. Met. 56 (2001) 375.
[117] J.C. Maxwell, Treatise on Electricity and Magnetism, third ed., Clarendon Press, Oxford, 1904.
[118] J.C. Maxwell-Garnett, Phil. Trans. Roy. Soc. London 203 (1904) 385.
[119] I.V. Belova, G.E. Murch, J. Metastable Nanocrystall. Mater. 19 (2004) 25.